2017-02-01

Facies Analysis, Sedimentary Petrology, and Reservoir Characterization of the Lower Triassic Sinbad Limestone Member of the Moenkopi Formation, Central Utah: A Synthesis of Surface and Subsurface Data

Kristopher Michael Powell
Brigham Young University

Facies Analysis, Sedimentary Petrology, and Reservoir Characterization of the Lower Triassic Sinbad Limestone Member of the Moenkopi Formation, Central Utah: A Synthesis of Surface and Subsurface Data

Kristopher Michael Powell

A thesis submitted to the faculty of
Brigham Young University
in partial fulfillment of the requirements for the degree of

Master of Science

Scott Ritter, Chair
Thomas Morris
Sam Hudson

Department of Geological Sciences

Brigham Young University

ABSTRACT

Facies Analysis, Sedimentary Petrology, and Reservoir Characterization
of the Lower Triassic Sinbad Limestone Member of the
Moenkopi Formation, Central Utah: A Synthesis
of Surface and Subsurface Data

Kristopher Michael Powell
Department of Geological Sciences, BYU
Master of Science

Lower Triassic strata in the Wellington Flat and Tully cores reflect a lateral transition from shallow water strata (Wellington Flats core) to strata that indicate deposition on a relatively more distal, storm-dominated ramp (Tully core). The Sinbad Member, along with the upper part of the underlying Black Dragon Member and the lower part of the overlying Torrey Member (Moenkopi Formation), are composed of ten carbonate, siliciclastic and mixed carbonate/siliciclastic facies deposited on a west-facing ramp/shelf that reached maximum flooding during Smithian time. Individual beds and facies display a large degree of lateral homogeneity and regional persistence in the study area.

The Wellington Flats core contains the three units characteristic of outcropping Sinbad Limestone: a basal skeletal unit, a middle peloidal unit, and an upper, oolitic dolomite unit. The more offshore Tully core is composed of skeletal grainstone, with fewer shallow-water carbonate and siliciclastic deposits. Discontinuity surfaces (hardgrounds, firmgrounds, and change surfaces) are common and indicate that sedimentation was punctuated by short-lived hiatuses accompanied by cementation, scour, and/or encrustation of the sediment-water interface. The Black Dragon, Sinbad, and lower Torrey Members represent at least one 3rd-order depositional sequence bounded below by the Tr-1 unconformity and above by lowstand deposits in the middle Torrey Member. Amalgamated fluvial channels in the middle of the Black Dragon Member may represent an additional 3rd-order sequence boundary that separates a Greisbachian sequence (lower Black Dragon Member) from the Smithian sequence (upper Black Dragon through lower Torrey members), but this is unsubstantiated by biostratigraphic data at present.

Diagenesis is strongly controlled by facies. Diagenetic elements include marine fibrous calcite cements, micritized grains, compaction, dissolution and neomorphism of aragonite grains, meteoric cements, pressure dissolution, and dolomitization. The paragenetic sequence progresses from marine to meteoric to burial. Marine and meteoric cements occlude much of the depositional porosity, which ranges from 0 to 10 % in the sample interval. The best reservoir qualities in core (1.0 md) occur in grainstones and quartz-siltstones. Although its relative thinness precludes it from being a major producer, the Sinbad Limestone Member of the Moenkopi Formation bears potential for modest future oil production.

Keywords: Moenkopi, Sinbad, Limestone, Reservoir Characterization, Facies, Petroleum, Stratigraphy, Sedimentology

ACKNOWLEDGEMENTS

I thank Whiting Petroleum Corporation and Larry Rasmussen for providing the funding for this research, as well as lending the two cores described in this paper. Without the physical cores and funding for thin sections, this research would never have been conducted or published.

This thesis would also not have been possible without the help of my advisor, Scott Ritter. His extensive knowledge of carbonate sedimentology and stratigraphy, pertaining specifically to the Sinbad Limestone, has been unparalleled and priceless. He has been willing to point me in the right direction and give me the necessary resources and advice needed to solve all of the problems I have encountered. His patience and cheerful nature has also made my research and time with him very enlightening and enjoyable.

I thank my other committee members, Tom Morris and Sam Hudson. Their counsel and knowledge of siliciclastic sedimentology has greatly aided my research. They also taught my undergraduate and graduate sedimentology courses, and helped me form the foundation of knowledge upon which I have continued to build.

My parents, Kraig and Kim Powell, have encouraged and nurtured my curiosity for the natural sciences throughout my entire life. I know that the many museum visits, vacations to national parks, and family hikes have helped foster my passion for learning about this world, and for that, I am forever grateful to them.

I thank my lovely wife, Allison Powell, for cheerfully following me on so many camping, hiking, and rock hounding trips in the two and a half years we have been married. She has never once complained about my ever-growing rock collection, and has been constantly supportive of my passions and goals. Finally, I thank my month-old son, Kaleb, for loving and supporting me, and bringing so much happiness into my life. I love you both so much, Allison and Kaleb.

TABLE OF CONTENTS

TITLE PAGE i
ABSTRACT ii
ACKNOWLEDGEMENTS iii
TABLE OF CONTENTS iv
INTRODUCTION 1
METHODS 2
SUMMARY OF PREVIOUS WORK 4
RESULTS 5
Lithostratigraphic Framework 5
Facies 12
Facies 1 – Fenestral-intraclastic dolomudstone 12
Facies 2 -Heterolithic siltstone/mudstone and nonskeletal packstone/mudstone 15
Facies 3 – Dolomudstone 19
Facies 4 – Ooid Grainstone 21
Facies 5 - Hummocky cross-stratified and laminated siltstone 22
Facies 6 – Peloidal Siltstone 24
Facies 7 – Skeletal grainstone to grain-dominated packstone 26
Facies 8 – Skeletal-peloidal wackestone to packstone 28
Facies 9 – Bioclastic-peloidal packstone 30
Facies 10 – Whole-bivalve-peloid packstone 31
Discontinuity Surfaces 33
Hardgrounds 33
Firmgrounds 34
Change Surfaces 35
Implications 35
Sequence Stratigraphy 41
Depositional History 45
Seafloor Diagenesis 49
Meteoric Diagenesis 49
Burial Diagenesis 50
Porosity and Permeability 55

CONCLUSIONS..... 58
REFERENCES 60

INTRODUCTION

The Sinbad Limestone Member (Moenkopi Formation) of east-central Utah has been the focus of many studies over the past 50 years because 1) it reflects the most widespread marine inundation of the western U.S.A. during Early Triassic time, 2) it was among the last marine carbonate units to be deposited on the Late Proterozoic to Early Triassic west-facing trailing margin of Laurentia, 3) it was deposited in seas decimated by the Permian-Triassic extinction, 4) and because it hosts modest amounts of oil and gas. As a result, Sinbad outcrops in the San Rafael Swell and Capitol Reef National Park have been studied by a large number of stratigraphers (REFS), paleobiologists (Pruss, etc, Bottjer), sedimentologists (Goodspeed and Lucas, 2007; Ritter et al., 2013; Olivier et al., 2016, and Olivier et al., 2016), biostratigraphers (Stephen et al., 2010; Brayard et al., 2015) and petroleum geologists (Lutz and Allison, 1992). Although the Sinbad has been thoroughly described and studied in outcrop, very little is known about the subsurface characteristics of this Member further west in central Utah. The purpose of this thesis is to correlate previously proprietary subsurface data with existing subsurface and outcrop data to develop a more complete understanding of the stratigraphic architecture, depositional patterns, diagenetic history, and reservoir character of the Lower Triassic Sinbad Member and parts of stratigraphically adjacent members.

METHODS

This study is based principally upon description and interpretation of two cores (Tully and Wellington Flats) of Lower Triassic Sinbad Limestone strata (Moenkopi Formation) collected from the subsurface in the vicinity of Price, Utah (Figure 1). The sampled interval in each core includes the Sinbad Member as well as adjacent parts of the Black Dragon and Torrey Members. Log and core data were provided by Whiting Petroleum of Denver, Colorado. Each core was described using the protocol developed by Bebout and Loucks (1984). Twenty-nine, blue-epoxy-impregnated thin sections were prepared from the Wellington Flats well, while 135 thin sections were prepared from the Tully well. The disparity in numbers of thin sections per core reflects incompleteness and relative homogeneity of the Wellington Flats core, relative to the more heterogeneous and more complete Tully core. A Nikon Eclipse 6400POL petrographic microscope was used for petrographic analysis. Multiple photomicrographs were taken of each thin section at different magnifications. Samples were then described and classified texturally according to Dunham (1962), Dott (1964), and Lucia (1995). Relative abundances of skeletal grains, non-skeletal grains, mud, and diagenetic components (porosity percent and types, cement, etc.) were determined for each thin section. Using a combination of texture, composition, and sedimentary structures, a set of facies was developed to best characterize and interpret the rock constituting the subsurface Sinbad Member and selected parts of adjacent members.

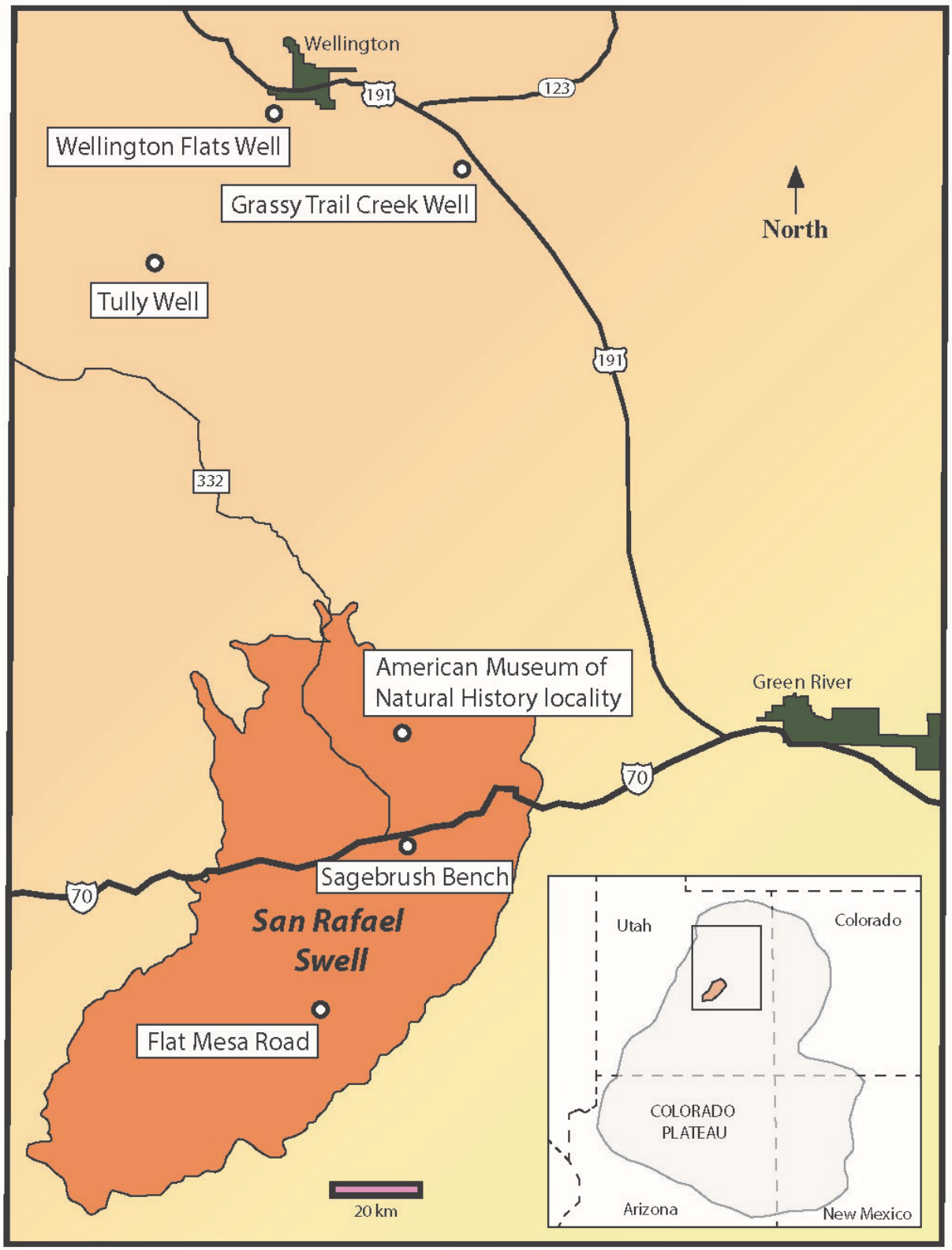

Figure 1. Location of core and outcrop used in this study. Wellington Flats and Tully cores were described, and description of the Grassy Trail Creek core and the three outcrops within the San Rafael Swell were used from Ritter and Osborne, 2013, to create the fence diagram in Figure 2.

SUMMARY OF PREVIOUS WORK

The Sinbad Limestone Member of the Moenkopi Formation was named by Gilluly and Reeside (1928) for relatively thin (15 to 25 meters) mesa-capping carbonates exposed in the crest ("Sinbad Country") of the San Rafael Swell, central Utah. The Sinbad was subsequently traced westward to the flanks of the Henry Mountains where Hunt (1953) recovered Lower Triassic ammonoids. During the 1960's, the Sinbad Limestone was mentioned only briefly in reports on the uranium potential and mineralogy of the Moenkopi Formation by Smith et al. (1963) and Hawley et al. (1968), respectively. The regional distribution and depositional environments of the Sinbad were described by Stewart et al. (1972) as part of their study of the Moenkopi Formation. In his more detailed studies of the Moenkopi in southeastern Utah, Blakey (1974, 1974) developed an informal tripartite (basal limestone- middle silty calcilutite-sandy dolostone cap) subdivision of the tidally-dominated Sinbad Limestone. Dean (1981) studied the depositional and diagenetic environments of the Sinbad in the Teasdale Dome located in and around Capitol Reef National Park, Utah. Batten and Stokes (1986) examined the numerous species of gastropods found in this Member in exposures in the San Rafael Swell, Utah. During the 1990's, one paper (Marzolf, 1993) and a few abstracts (Porter, 1991, Lutz, 1993, and Goodspeed and Elrick, 1993) discussed the sequence stratigraphy of the Sinbad specifically and the Moenkopi Formation in general. During the next two decades, Sinbad studies focused mainly on post-extinction faunal diversity and biotic recovery, including papers by Schubert and Bottjer (1995), Twichett et al. (1995), Fraiser and Bottjer (2000, 2004), Boyer et al. (2004), Nutzel and Schulbert (2005), Hautmann and Nutzel (2005). In the last decade there has been a resurgence of sedimentological and biostratigraphic studies of early Triassic strata in Utah and parts of

adjacent states (Goodspeed and Lucas, 2007; Stephen et al., 2010; Brayard et al., 2013; Ritter et al., 2013; Oliver et al., 2014; Oliver et al. 2016.

Relative to petroleum potential, the Sinbad produced oil from a 445 foot-long lateral in the Grassy Trail Creek located on the north-plunging nose of the San Rafael Swell (Figure 1). Lutz and Allison (1992) identified two carbonate lithofacies in core: cross-bedded oolite and skeletal wackestone to packstone. Oolitic shoal sands (up to 8 meters thick) contain minor intraparticle porosity related to preferential dolomitization of ooids and intergranular (interooid) porosities of 10%. Measured permeability ranges from 0.52 to 0.88 md with 20% oil saturation (Lutz and Allison, 1992; Allison et al., 1993). Skeletal wackestones and packstones have measured porosities of 1 to 2% and permeabilities ranging from 0.01 to 0.02 md. 15 to 30 MMCFG were produced from the Sinbad Limestone between 2,725 and 2,755 feet in the Last Chance South field located on the southwestern flank of the San Rafael Swell in southwestern Emery County, Utah (Jackson, 1993). In their summary of oil and gas exploration in Carbon, Emery, and Sanpete Counties, Laine and Staley (1991) listed evaluation of the Moenkopi reservoirs using horizontal drilling techniques as a recommended target for future exploratory efforts.

RESULTS

Lithostratigraphic Framework

In the study area and adjacent outcrop belt, Lower Triassic strata are assigned to the Black Dragon, Sinbad, Torrey, and Moody Canyon Members (Moenkopi Formation) (Figure 2). The Black Dragon Member varies in thickness from tens of centimeters at its southern pinchout to 150 meters in thickness in east-central Utah (Ochs and Chan, 1997) as a function of variable accommodation resulting from uneven (>20 meters) incision of the upper Black Box (Kaibab)

Dolomite (Orgill, 1974) during the 24 million year-long hiatus that marks the Permian-Triassic system boundary in this area. Ochs and Chan (1997) subdivided the Black Dragon Member into five stratigraphic-depositional units, which are (in ascending order) a basal channelized chert-pebble conglomerate, lower siltstone and shale unit, cross-bedded sandstone complex, upper siltstone and shale unit, and member-capping peritidal dolomite interval. This informal subdivision of the Black Dragon is recognized and followed herein.

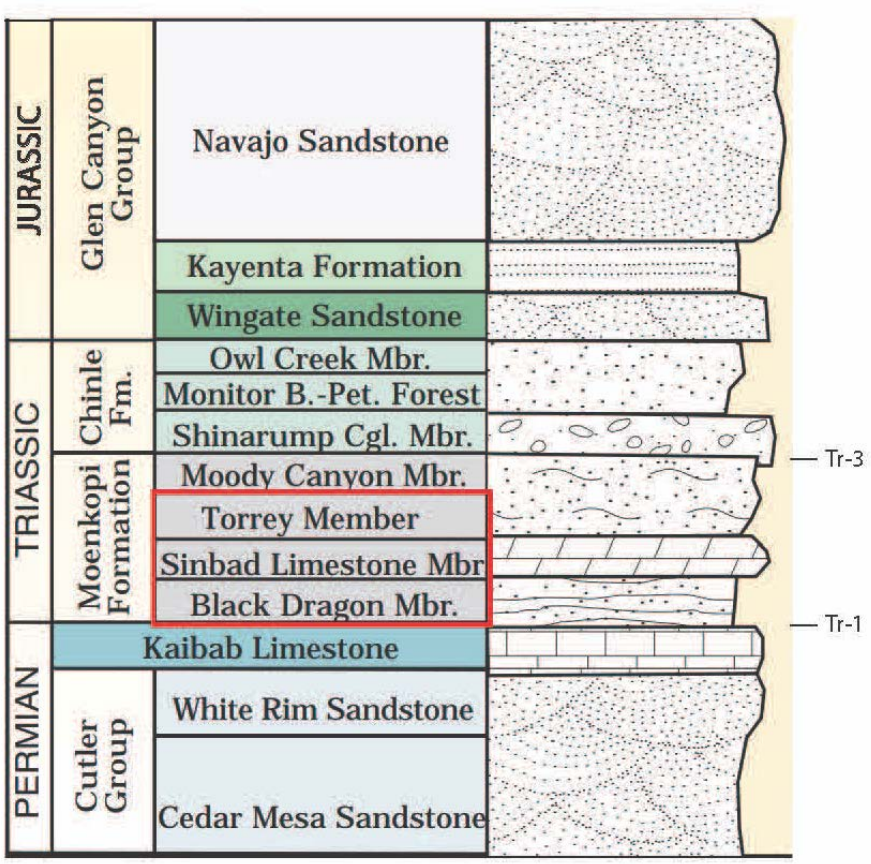

Figure 2. General stratigraphic column of Central Utah near the San Rafael Swell. Members of the Moenkopi Formation specifically described in this paper are outlined in red. Tr-1 and Tr-3 represent the first and third Triassic unconformities, respectively. Modified from Mathis, 2000.

As first noted by Blakey (1973, 1974), the Sinbad Member in east-central Utah is readily divisible into three informal units, a basal limestone, and medial silty-peloidal unit, and a dolomitized, nonskeletal, oolitic capping unit. These units were further described and interpreted

by Goodspeed and Lucas (2007) and by Ritter et al. (2013). This tripartite subdivision is recognizable in the Grassy Trail Creek core (Lutz and Allison, 1992), Wellington Flats core, and Tully core (this report), but the three units are somewhat different in the relatively deeper-water strata of the Tully core (Figure 3). In the Tully Core, the bottom unit is comprised mostly of skeletal limestone, with some dolomitized mudstone beds. The middle unit still is mostly siltstone, but contains skeletal grainstone intervals. The uppermost unit consists almost wholly of skeletal limestone, instead of oolitic grainstone, as is seen in outcrop to the Southeast and in more eastward cores. Very few ooids were observed in the upper unit of the Tully core.

The Black Dragon-Sinbad contact is drawn at the transition from dolomitic tidal and peritidal strata (peritidal dolomite facies/unit of Ochs and Chan, 1997) to skeletal limestone of the basal Sinbad Member in the Wellington Flats and Tully cores (Figure 4, Figure 5, and Figure 6). The contact between the Sinbad and superjacent Torrey Member is historically drawn at the transition from medium- to thick-bedded, dolomitized carbonate grainstone to thin bedded, siltstone and shale with minor carbonate components. This protocol is followed herein, although it must be noted that the lower part of the Torrey Member in the Tully core contains variable admixtures of carbonate grains, chiefly peloids in the basal siltstone beds and that skeletal carbonates and mixed nonskeletal-quartz silt units occur for several tens of meters into the lower Torrey Member (Figure 4), in contrast to the predominantly siliciclastic facies comprising the Torrey Member in the San Rafael Swell and Capitol Reef outcrop belts.

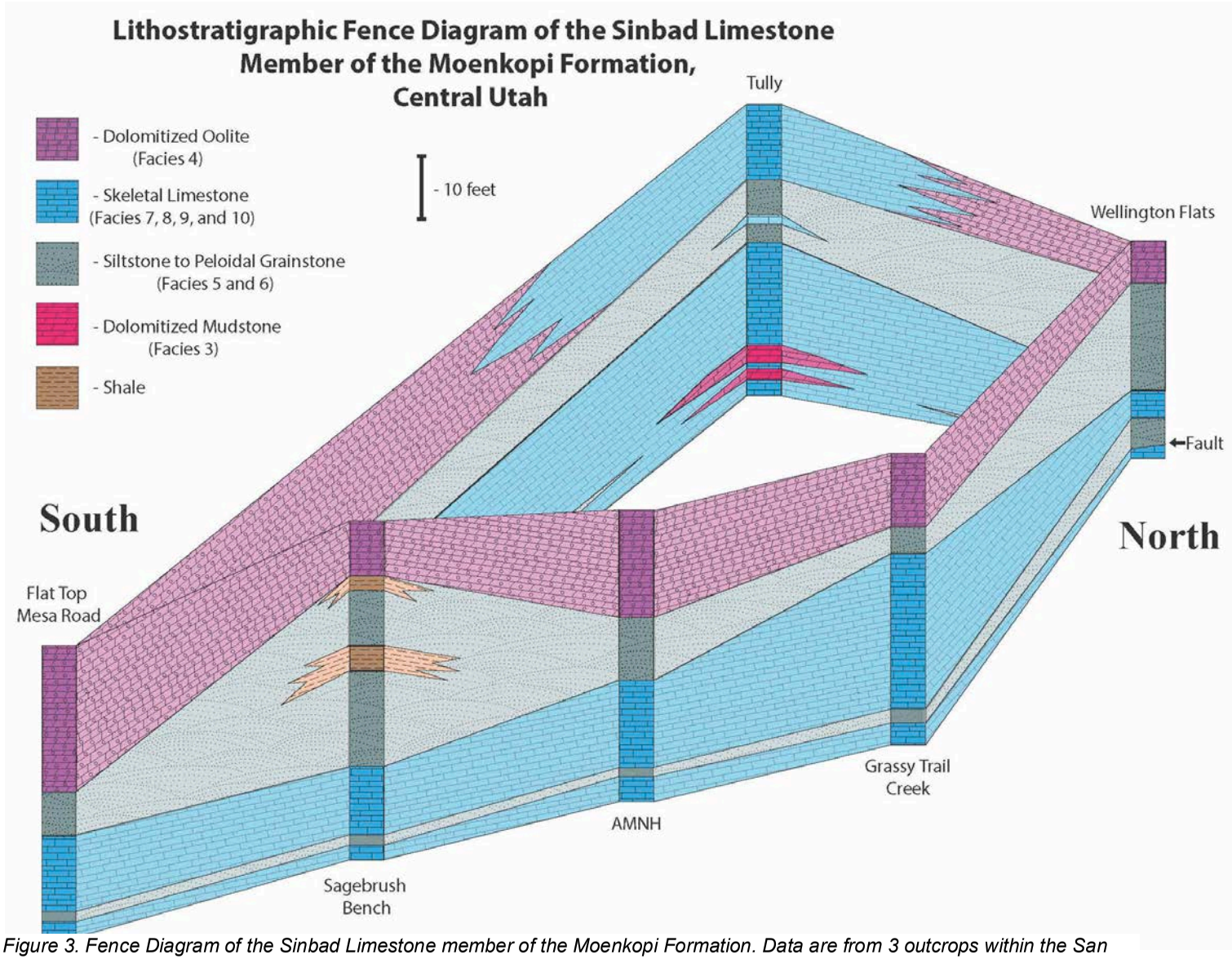

Figure 3. Fence Diagram of the Sinbad Limestone member of the Moenkopi Formation. Data are from 3 outcrops within the San Rafael Swell (Flat Top Mesa Road, Sagebrush Bench, and AMNH [American Museum of Natural History locality]), and 3 cores from north of the San Rafael Swell (the Tully core, the Wellington Flats core, and the Grassy Trail Creek core

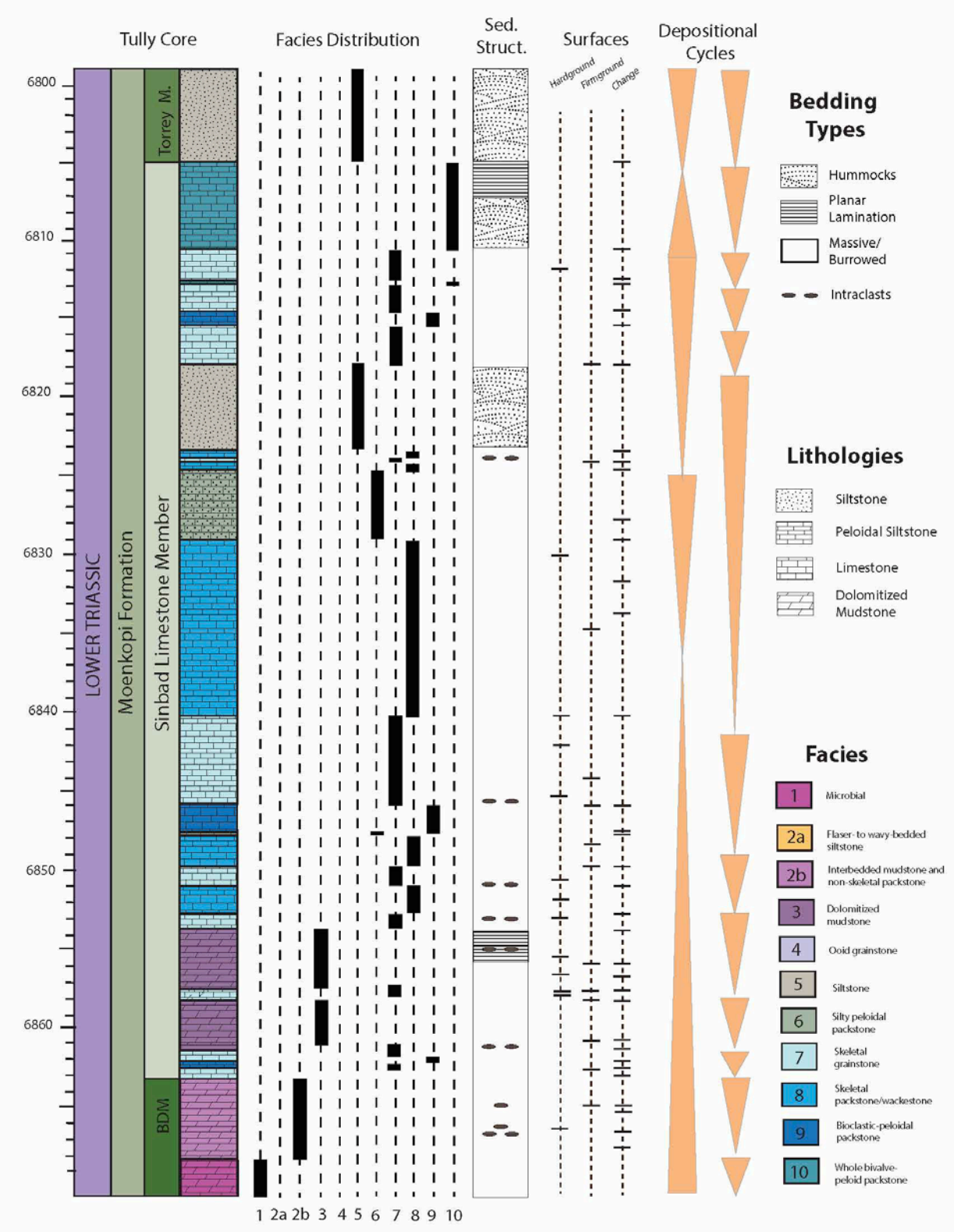

Figure 4. Stratigraphic column of the Sinbad Limestone in the Tully core, showing facies distribution, sedimentary structures, discontinuity surfaces, and depositional cycles. For depositional cycles, cycles on left represent high order sequences, with low order sequences on the right.

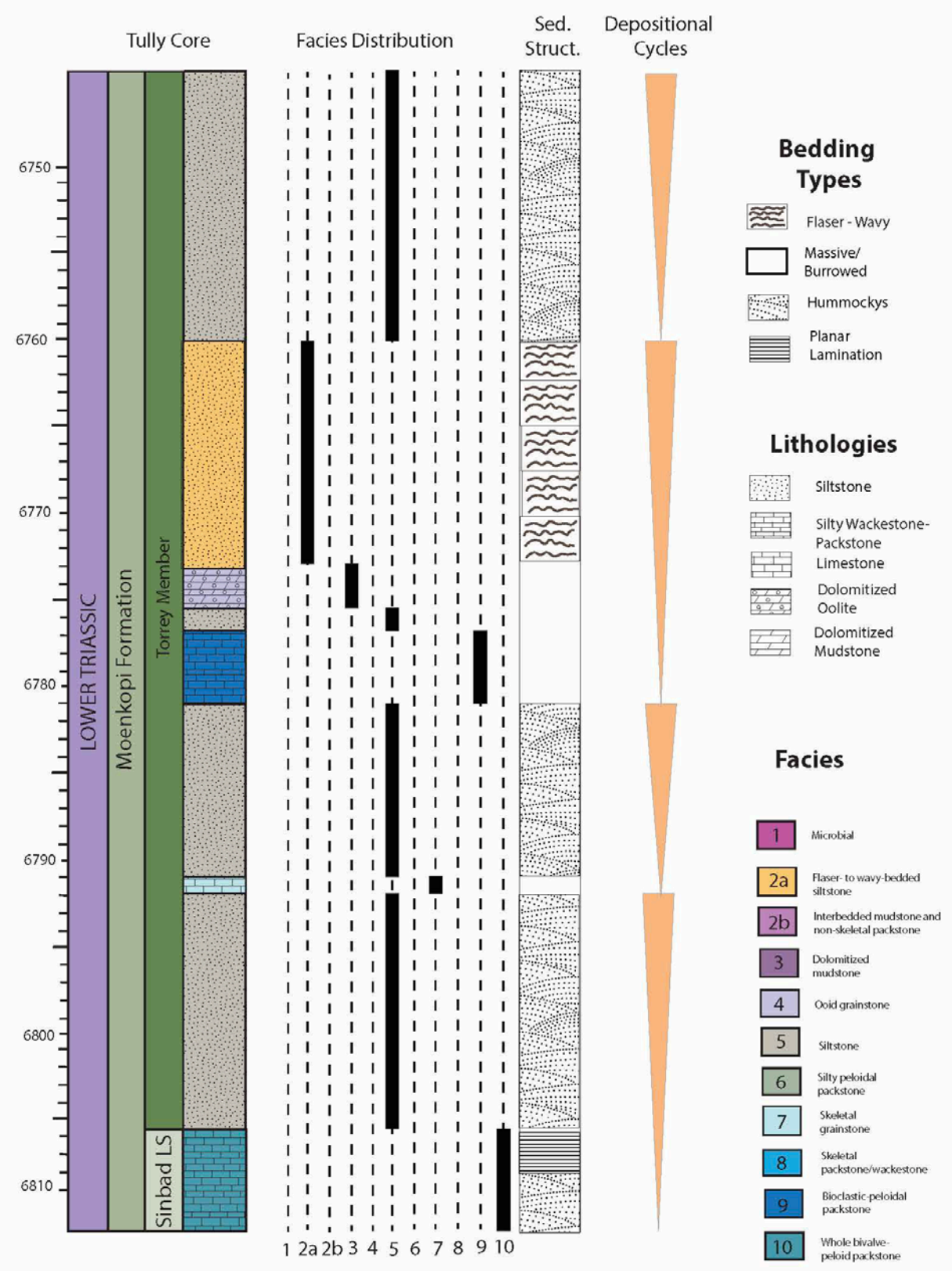

Figure 5. Stratigraphic column of the lower Torrey Member in the Tully core, showing facies distribution, sedimentary structures, and depositional cycles. Depositional cycles represent high order sequences.

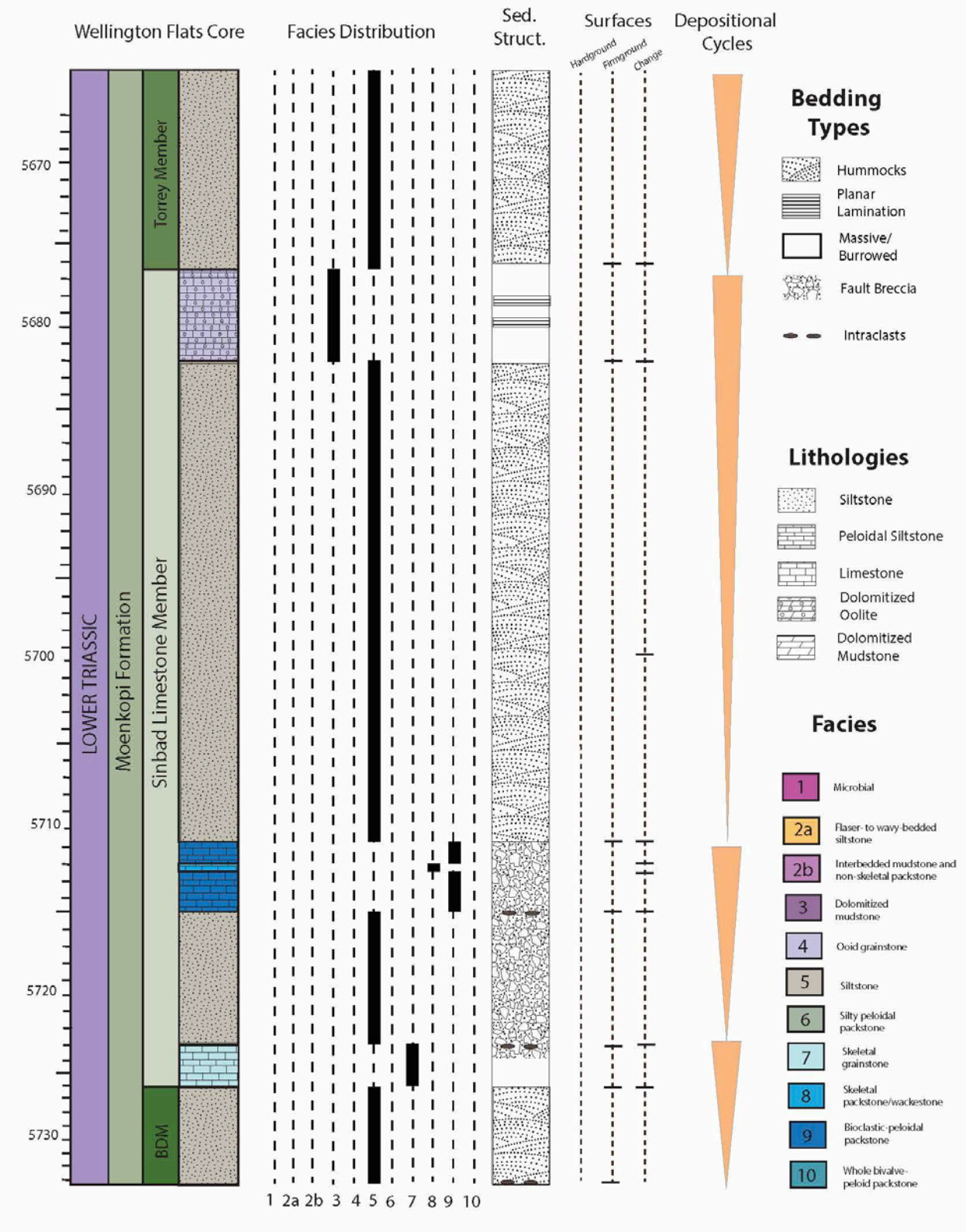

Figure 6. Stratigraphic column of the Sinbad Limestone in the Wellington Flats core, showing facies distribution, sedimentary structures, discontinuity surfaces, and depositional cycles. Depositional cycles represent high order sequences.

Facies

In core, the Sinbad Limestone Member is a mixed carbonate-siliciclastic succession comprised of a low-diversity skeletal and nonskeletal grain association and peloidal quartz siltstone. Bivalves and micrograstropods, and to a lesser extent crinoids, ophiuroids, scaphopods, ostracodes, and worm tubes are the dominant fossil components. This facies suite is indicative of deposition on a storm-dominated carbonate ramp similar to those described from other Lower Triassic platforms in the wake of the Premian-Triassic extinction (Twitchett, 1999; Lehrmann, 2006). These facies are described below in an onshore to offshore progression. Key attributes of these facies are summarized in Table 1.

Facies 1 – Fenestral-intraclastic dolomudstone

Although rare, this supratidal facies is a critical indicator of shoreline position in the Tully core. The facies is composed of interbedded peloidal wackestone to mud-dominated packstone with fenestrae and thin, vertical sheet cracks (light-colored areas in Figure 7b), alternating with skeletal-peloidal-intraclastic grainstone (dark areas in Figure 7b). Contacts between these two rock types are irregular with several centimeters of relief visible in some cases. Laminated bedding accentuated by thin, spar-filled sheet cracks is typical of the peloidal wackestone lithology. Undulatory or domal bedding is present in core (Figure 7). Though present, skeletal grains comprise a minor constituent of wackestone beds.

The interbedding of matrix- and grain-rich facies derives from deposition in a supratidal setting that was intermittently affected by storm surges. The laminated, peloidal wackestone to mud-dominated packstone reflects ambient spring-tidal delivery of peloids and skeletal grains to

the supratidal flat where they were bound by microbial activity (as indicated by presence of undulatory laminations and fenestrae). Grain-rich interbeds and irregular contacts indicate events of increased energy, possibly storm surge, when grain sorting, scouring of the upper few centimeters of the depositional surface, and emplacement of intraclasts were the dominant depositional processes. The microbial laminae and fenestral fabric of this facies suggests that it is a supratidal microbial deposit. In supratidal enrivonments, microbial mats can thrive, without predators to destroy them.

Facies Number	Facies name	Predominant Lithology	Grain Types	Sedimentary Structures	Depositional Environment
Facies 1	Microbial	Dolomite	Carbonate mud	Microbial laminae	Supratidal
Facies 2a	Flaser- to wavy-bedded siltstone	Quartz siltstone	Quartz silt	Flaser bedding, wavy bedding	Tidal
Facies 2b	Interbedded mudstone and non-skeletal packstone	Dolomite	Intraclasts, carbonate mud	laminae, burrows	Tidal
Facies 3	Dolomitized mudstone	Dolomite	Carbonate mud, quartz silt	Massive, burrows	Lagoon
Facies 4	Ooid grainstone	Dolomite	Ooids, silt sized quartz grains	Cross bedding	Ooid shoal
Facies 5	Siltstone	Quartz siltstone	Silt sized quartz grains, peloids	Hummocks	Deeper restricted shelf
Facies 6	Peloidal siltstone	Quartz siltstone	Silt sized quartz grains, peloids	Massive, burrows	Restricted shelf
Facies 7	Skeletal grainstone	Limestone	Bivalves, gastopods, echinoderms, scaphopods, quartz silt, peloids	Massive, burrows	Skeletal rich shoals
Facies 8	Seletal wackestone to packstone	Limestone	Bivalves, gastopods, echinoderms, scaphopods, quartz silt, peloids, mud	Massive, burrows	Well circulated, shallow sub tidal
Facies 9	Bioclastic packstone	Limestone	Bivalves, gastopods, echinoderms, scaphopods, quartz silt, peloids	Burrows	High energy shoreface
Facies 10	Whole bilvalve-peloid packstone	Peloids	Peloids	Massive, hummocks	Distal Ramp

Table 1. Description of facies found within the Sinbad Limesone in the Tully and Wellington Flats cores.

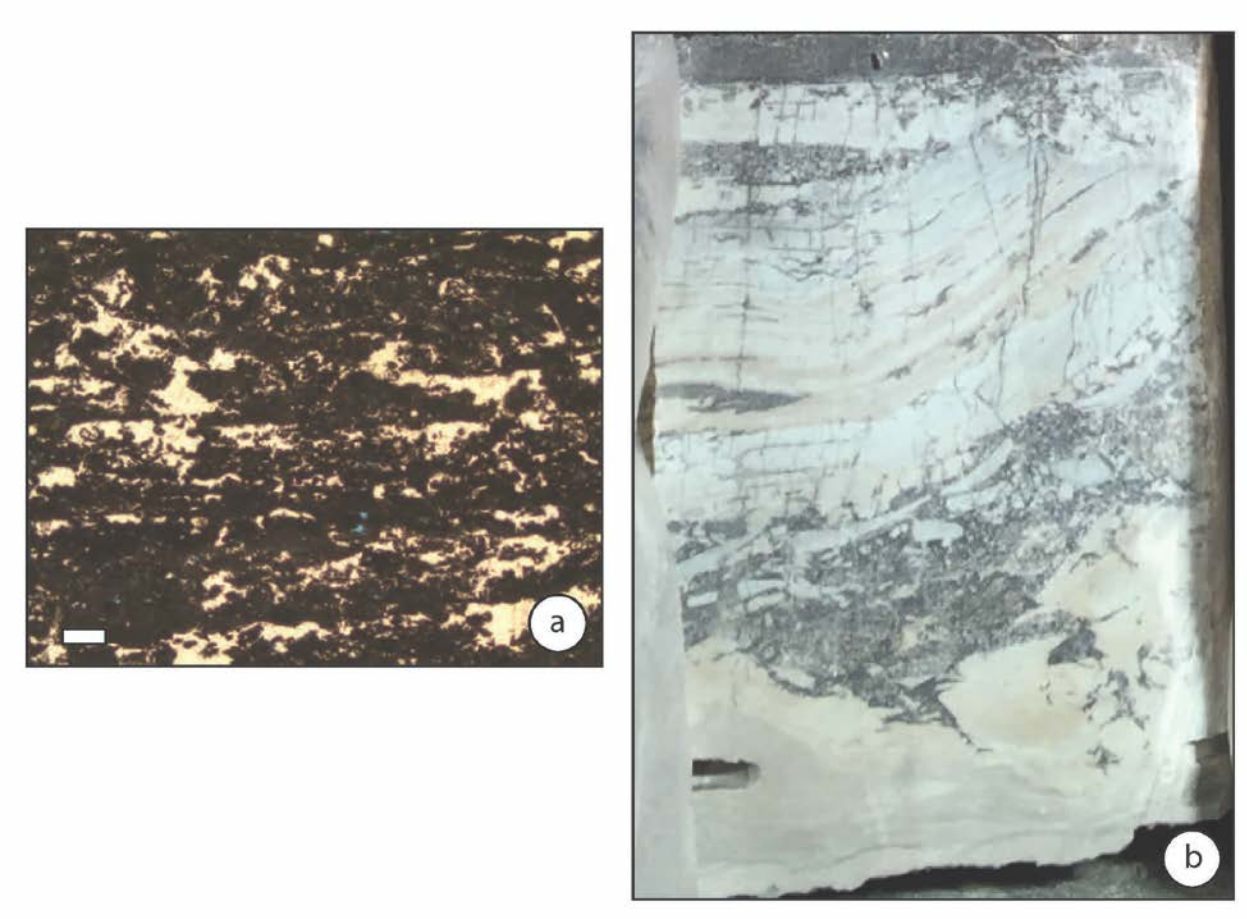

Figure 7. Photomicrographs and core showing examples of facies 1. a) is a photomicrograph of a fenestral mudstone in the Sinbad Limestone found in outcrop within the San Rafael Swell from Ritter et al, 2007. Scale bar is 0.5 mm. b) sample from 66869.0 to 6869.6 ft in the Tully core showing interbedding of muddy (light color) and grain-rich (dark areas) with mud intraclasts. Tilted bedding overlying the intraclastic horizon is part of a domal stromatolite.

Facies 2 -Heterolithic siltstone/mudstone and nonskeletal packstone/mudstone

This tidalite facies is divided into mixed carbonate-siliciclastic (2a) and predominantly carbonate (2b) subfacies.

Facies 2a - Flaser- to wavy-bedded siltstone and mudstone

Facies 2a is characterized by a heterolithic interbedding of silt and mud that ranges from flaser to wavy. The silt component is predominantly angular monocrystalline quartz with subordinate amounts of peloids, micro-ooids, and mica that appear dark in core slabs (Figure 8).

Muddy interbeds are light greenish gray in color on core slabs (Figure 8), and are comprised of dense mud with sparse flecks of quartz silt and mica. Contacts between silt and mud interbeds are typically sharp, and ripples are symmetrical. Silt packages are usually flat-bottomed with undulose upper surfaces. Scoured contacts are also in evidence resulting in removal of muddy interbeds and production of angular mudclasts that float in siltstone matrix. This facies formed in response to alternations in current velocity and sediment supply and is interpreted to reflect deposition in the intertidal zone. At 6767 feet in the Tully core, the muddy layers that drape sand ripples were rich in organic material that has been compacted to form wispy seams between the silty interbeds (Figure 8).

The heterolithic flaser- and wavy-bedding present in this facies is typical of tidal environments. The variable direction and energy of ebb and flood tidal currents is considered to cause deposition to alternate between silt and mud particles (Reineck & Wunderlich, 1968; He and Gao, 1999).

Facies 2b – Interbedded mudstone and non-skeletal packstone

This facies is comprised of alternating domains of light-colored, dolomitized carbonate mudstone and dark-colored, nonskeletal wackestone and packstone (Figure 9). Textural domains (beds) range from a few millimeters to a few centimeters in thickness. Boundaries between domains may be sharp where individual laminations or thin beds are preserved. However, most boundaries are irregular and diffuse with grain-filled burrows invading muddy domains and vice versa. Domains may or may not be laterally persistent, even across the width of a core slab. The grain association includes variable percentages of ooids, peloids, and intraclasts (Figure 9). Skeletal grains occur only rarely. These facies is found in the uppermost Member of the Black Dragon Member in the Tully core from 6863.5 feet to 6869 feet.

Like Facies 2a above, this facies is interpreted to reflect deposition under fluctuating hydraulic conditions. Unlike the siliciclastic tidal flats where physical processes controlled bedding, however, carbonate tidal flat deposits of Facies 2b reflect a combination of physical and biological processes operating in the depositional environment. Burrowers inhabited the tidal flats, but their activity was not so pervasive that primary bedding was completely destroyed.

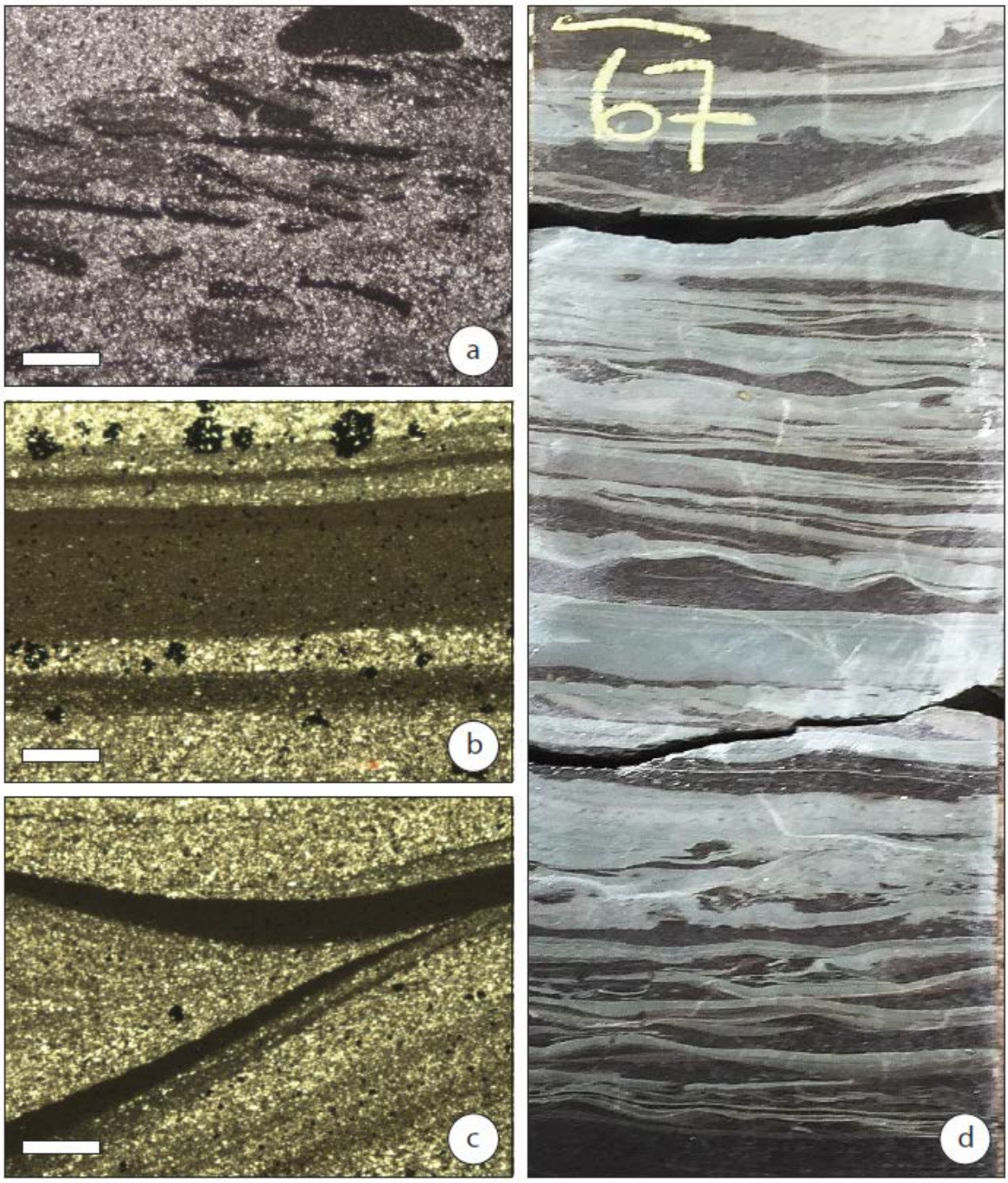

Figure 8. Photomicrographs and core slab of the Tully core showing examples of facies 2a. a) Disrupted mud laminae, 6736 ft, b) Horizontal interbeds of mud and quartz silt, 6767.5 ft , c) Mud draped ripples, 6769.9 ft, d) Core slab of facies 2a from 6767 ro 6767.9 ft. Light colored intervals are mud. Dark intervals are quartz-rich siltstone. Scale bar on thin-section photomicrographs is 0.5 mm.

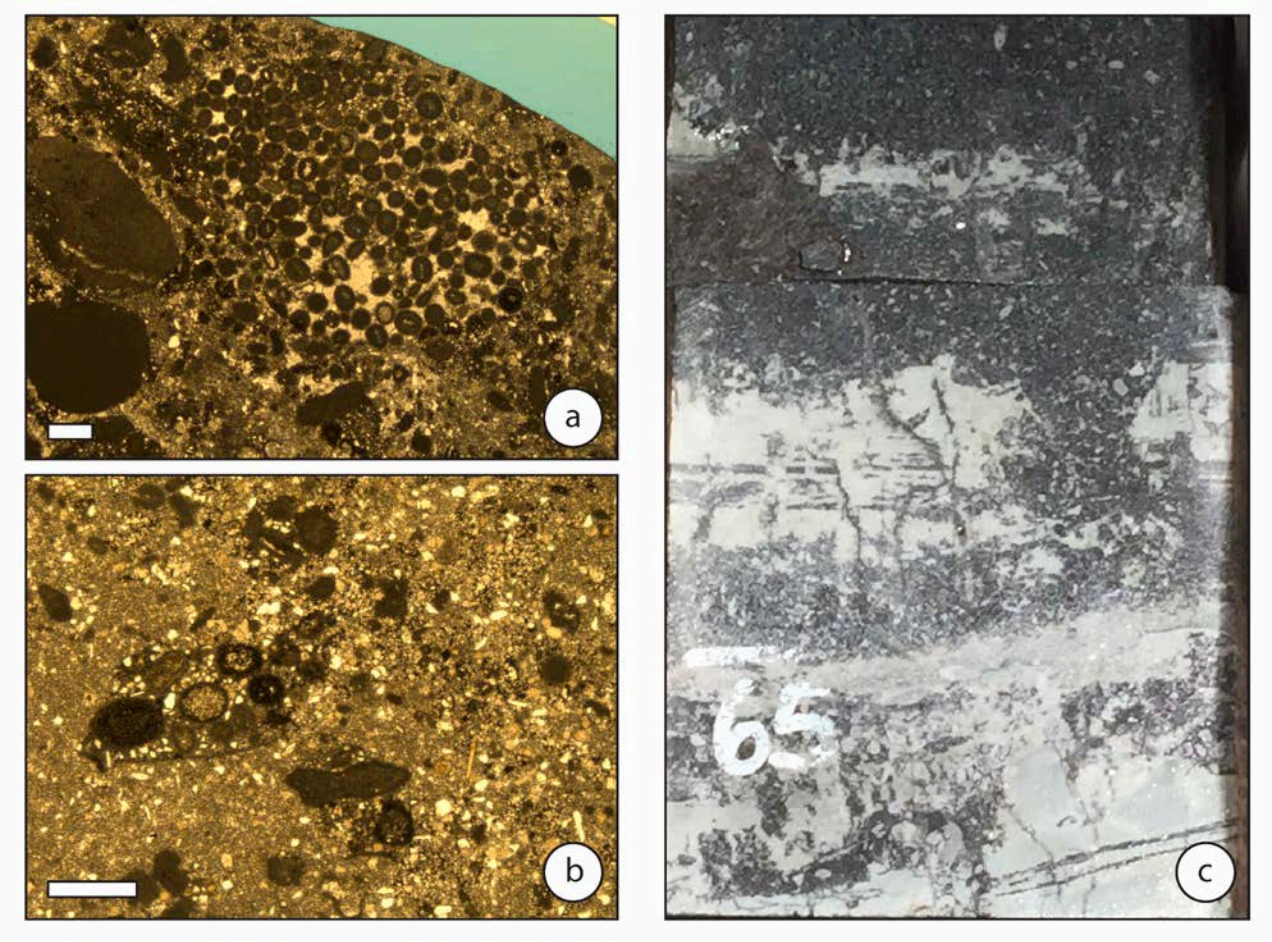

Figure 9. Photomicrographs and core slab from the Tully core showing examples of facies 2b. a) Nonskeletal packstone, 6865 ft, b) Nonskeletal wackestone, 6864.6 ft, c) Alternating mudstone (light colored) and grainstone (dark colored) interbeds, 6864.7 to 6865.2 ft. Scale bar for thin-section photomicrographs is 0.5 mm.

Facies 3 – Dolomudstone

These carbonate rocks are almost wholly comprised of dolomitized carbonate mud. Little or no calcite may be present (as indicated by red calcite stain). Small peloids, rare bioclasts, and quartz silt form minor constituents of this facies. Bedding ranges from laminated to massive. The dolomite fabric is unimodal, finely crystalline and fabric retentive, preserving bedding and burrows. Dolomite crystals are mostly planar, subhedral rhombs (planar-s), with planar

boundaries and little or no microporosity between crystals (Figure 10). Rocks of this facies occur between 6853.3 and 6866.6 feet of depth in the Tully core.

Based upon the muddy nature of the rocks, near absence of skeletal grains, preservation of internal bedding, and vertical facies relationships, we conclude that this facies was deposited in the inner ramp lagoon, basinward of the tidal belt and shoreward of high-energy mid-ramp shoals. The absence of skeletal grains and preservation of laminations indicates that the lagoonal waters were generally inimical to epifaunal and infaunal organisms.

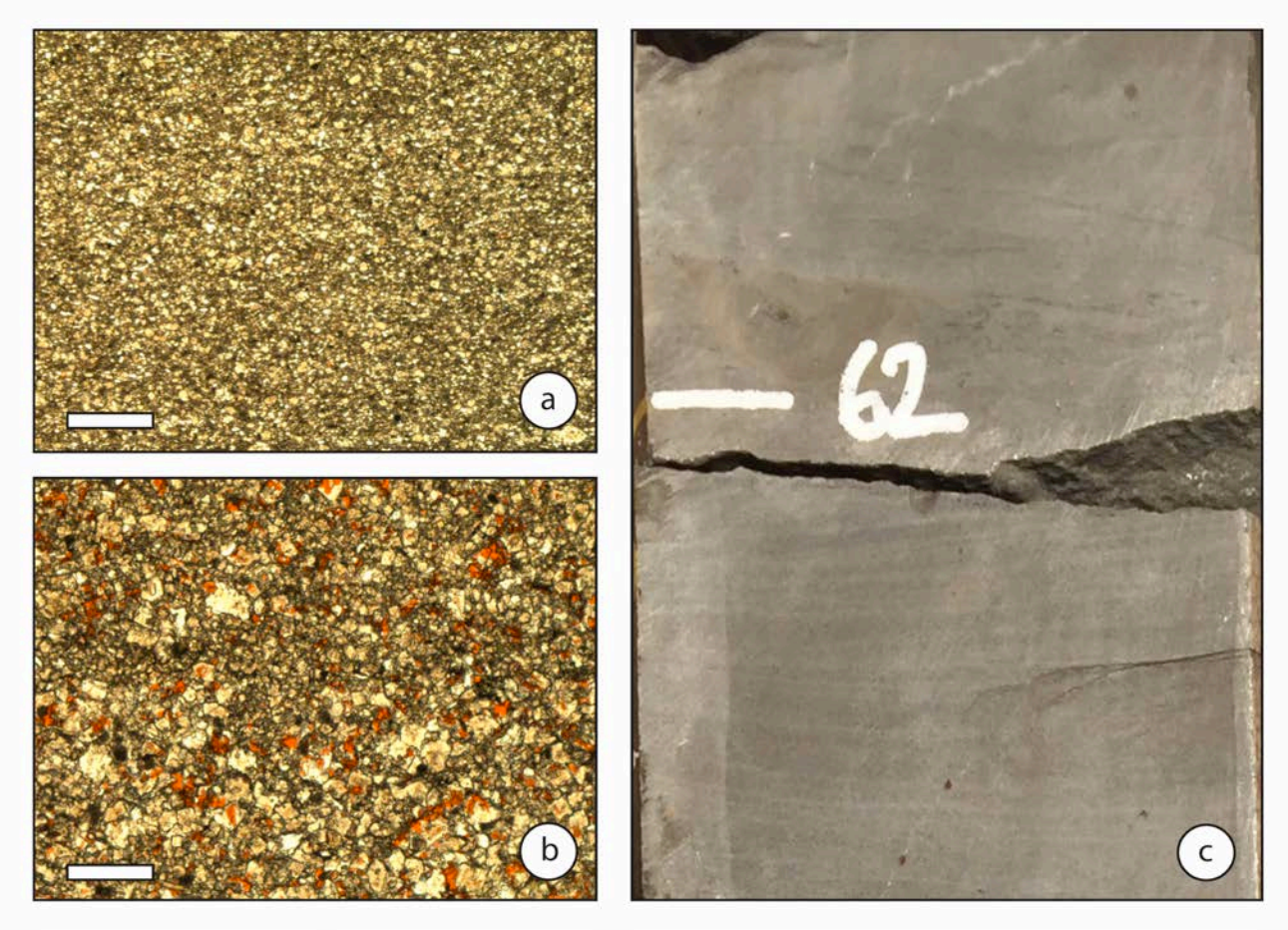

Figure 10. Photomicrographs and core slab image from the Tully core showing examples of Facies 3. a) 6859 ft, b) 6862 ft, c) 6862 ft. Images from Tully core. Core slab shows massive and planar laminated dolomitized mudstone. Scale bar on photomicrographs is 0.5 mm

Facies 4 – Ooid Grainstone

This grain-dominated facies is composed chiefly of ooids (75-90%) with complementary percentages of peloids, intraclasts, and skeletal grains. Ooids range from 30 to 70 microns in size. Peloids and rounded quartz grains compose the majority of nuclei. Micritization and has obscured the cortical structure of most ooids, however, tangential fabrics prevail where cortical structure has been preserved (Figure 11). Moderately well sorted textures prevail. In the Wellington Flats core, this facies contains 10-25% quartz silt. This facies comprises the upper Member of the Sinbad Member (between 5676.5 and 5682 feet) in the Wellington Flats core. In the more offshore Tully core, it is absent in the Sinbad Member, but constitutes a small stratigraphic interval (between 6773 and 6776 feet) in the Torrey Member. In both cases, this facies occurs above hummocky cross-stratified, peloidal siltstone to silty peloidal grainstone and represents shoaling conditions.

Rocks of this facies have been largely dolomitized. The dolomite fabric is unimodal, finely crystalline and fabric retentive, preserving cortical structure if not previously obscured by micritization. Dolomite crystals are mostly planar, subhedral rhombs (planar-s), with planar boundaries and little or no microporosity between crystals.

The texture, composition, and stratigraphic relationships to underlying facies indicate that deposition took place above fairweather wave base in shoaling seas. Cross bedding that is visible in the core is indicative high energy shoals. Farther updip, in the San Rafael Swell outcrop belt, oolitic grainstones display herringbone cross bedding indicating final deposition of shoal-derived coated grains in the updip tidal belt.

Facies 5 - Hummocky cross-stratified and laminated siltstone

This dominantly siliciclastic facies consists of medium gray, hummocky cross-stratified (HCS) peloidal siltstone (Figure 12). Grains are primarily well-sorted monocrystalline quartz with admixtures of small carbonate grains, muscovite flakes, and traces of feldspar. Grain size ranges from coarse silt to very fine sand (50 to 100 microns in diameter) and quartz grains are typically angular to subangular. This facies contains from 10 to 30% calcareous material in the form of small peloids, microbioclasts, small (50 to 75 micron) dolomite rhombs, and micro-ooids. Interstices between grains are filled with opaque iron oxides, bitumens, and sparry calcite cement. The scale of the HCS is difficult to measure in core, but updip outcrop analogs range from 0.5 to 2 meters in length and from 0.1 to 1.5 meters in thickness. In core slabs, HCS typically presents as horizontal or gently inclined planar laminated bedding. Discordant erosional contacts between bed sets and convex-up bed morphologies are evident in some core horizons.

The texture and hummocky bedding of this facies indicates deposition on the offshore, storm-wave-swept portion of the Sinbad shelf. Absence of burrowers (and preservation of bedding) was a function of low nutrient levels in the sediment and/or frequent reworking of seafloor sediment that discouraged colonization. This facies occurs between 5856 and 6853.5 and between 6805 and 6778 feet in the Tully core. HCS is prevalent between 5708 and 5691 feet in the Wellington Flats core. The quartz silt was delivered by wind and streams to the eastern shoreline of the Sinbad shelf. The source of the quartz and mica was the greatly reduced remnant of the Uncompaghre uplift, which was located tens of miles to the east in the vicinity of modern-day western Colorado (Blakey, 1974).

The lack of larger, angular grains suggests that this facies was deposited below wave base. However, the hummocky cross stratification present in the core indicates that this facies

was deposited above storm wave base, as storms likely deposited the hummocks of sediment. The lack of carbonate sediment and clasts from coral or shells suggests either that the environment was too deep, or there was too much incoming sedimentation to support an adequate carbonate factory during these intervals.

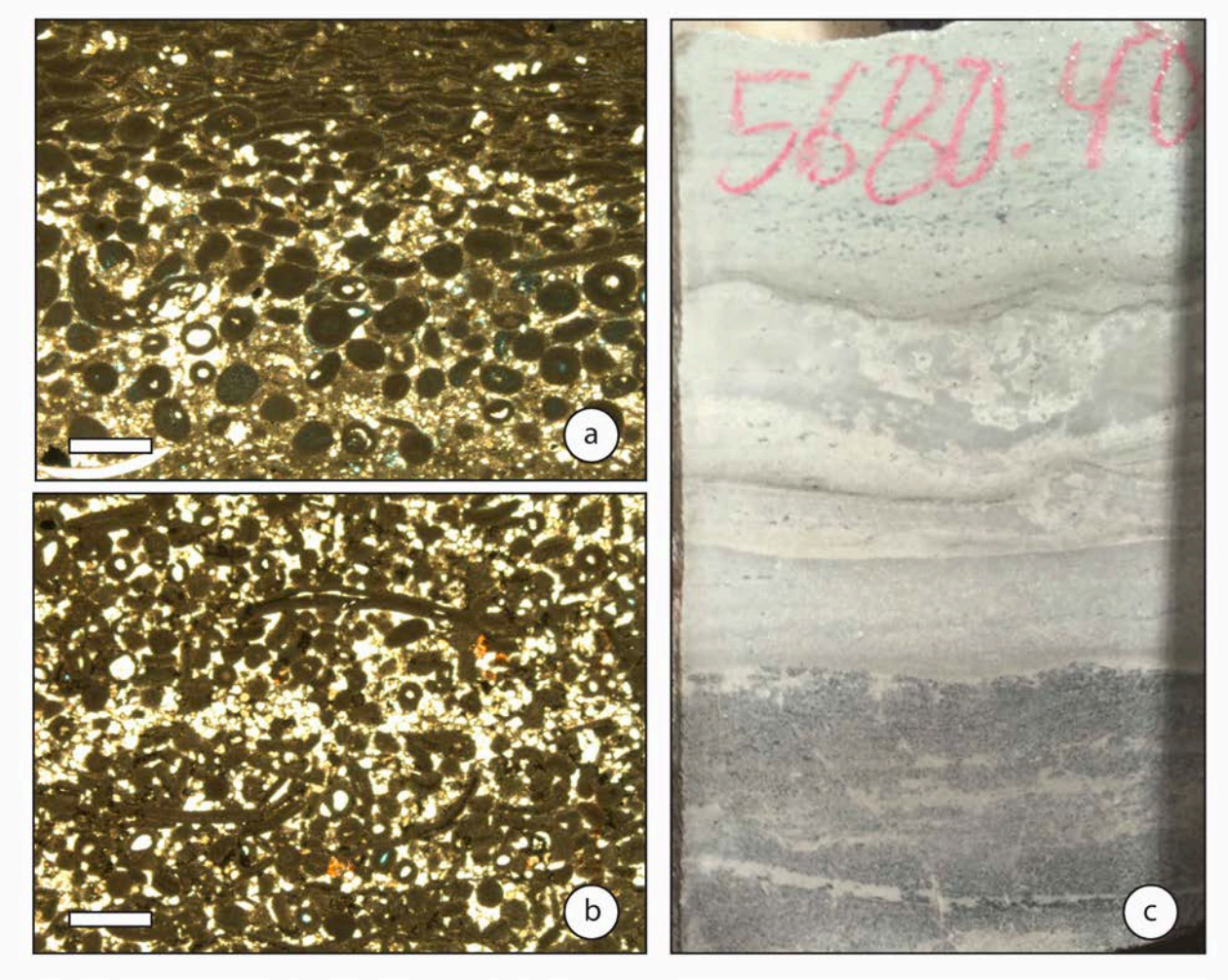

Figure 11. Photomicrographs and core showing examples of facies 4. a) 5680.5 ft, b) 5679 ft, c) 5680.4 ft. Images from Wellington Flats core. Core slab shows oolitic facies in the lighter, upper two thirds of the slab photograph. Note compaction of ooids in a). Scale bar on photomicrographs is 0.5 mm.

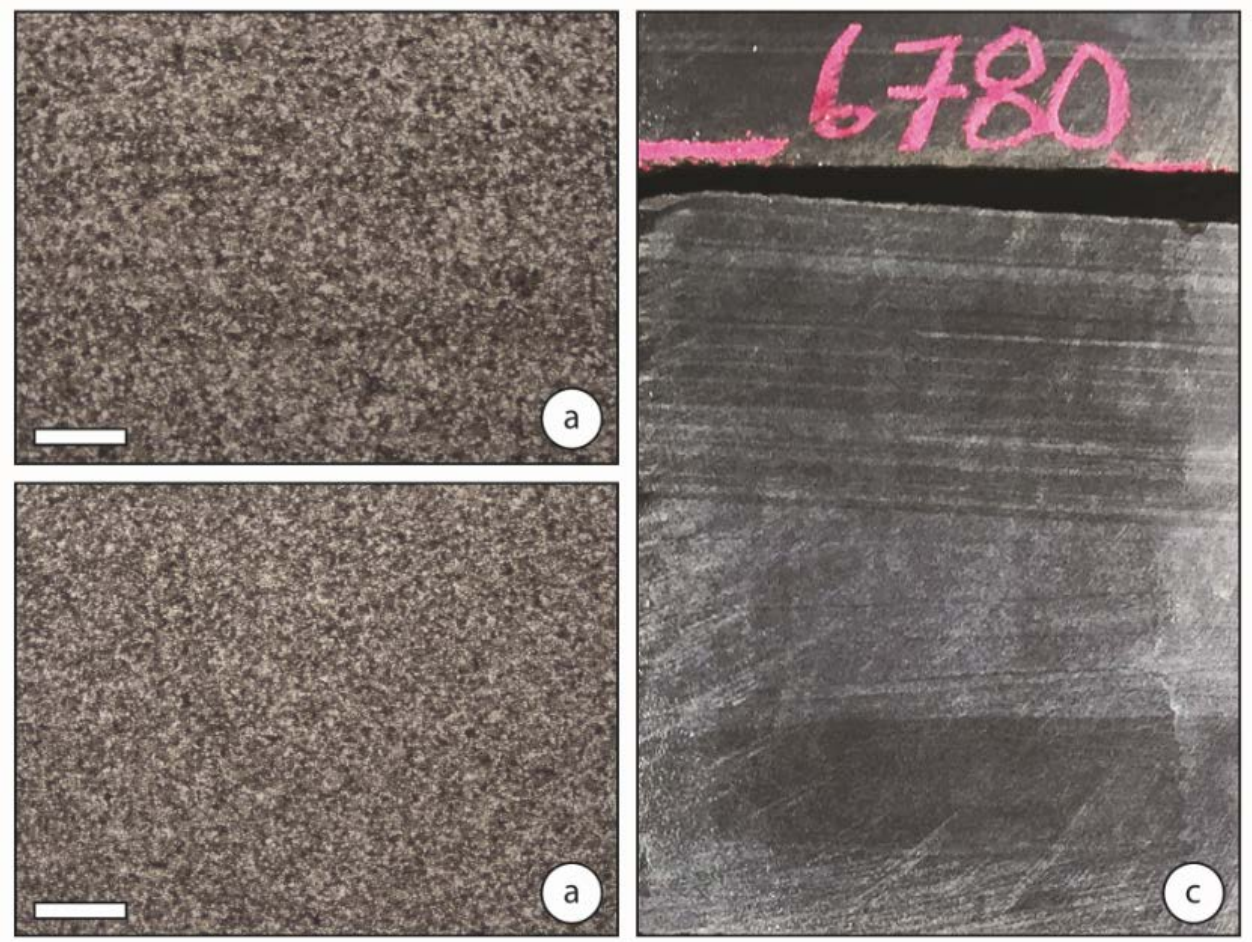

Figure 12. Photomicrographs and core showing examples of facies 5. a) 6782 ft, b) 6790 ft, c) 6780 ft. Images from Tully core. Core slab shows planar lamination in the upper half and hummocky cross-stratification in the lower half. Scale bar on photomicrographs is 0.5 mm.

Facies 6 – Peloidal Siltstone

This facies contains mostly peloids, with quartz silt (Figure 13a). The higher percentage of peloids than found in the siltstone facies indicates a more active carbonate factory, and likely lower rates of siliciclastic sedimentation. Some sections also have micro-ooids. Peloids make up between 50-75% of this facies. Bedding ranges from ripple cross-laminated (Figure 13b) to massive. This facies occurs between 6824.8 and 6829 feet in the Tully core.

The high percentage of peloids in this facies indicates an active carbonate factory nearby, but the influx of quartz silt precluded development of a vigorous skeletal carbonate factory in the location of the Tully core. This facies was deposited in a similar environment to facies 5, but further down ramp, with lower energy.

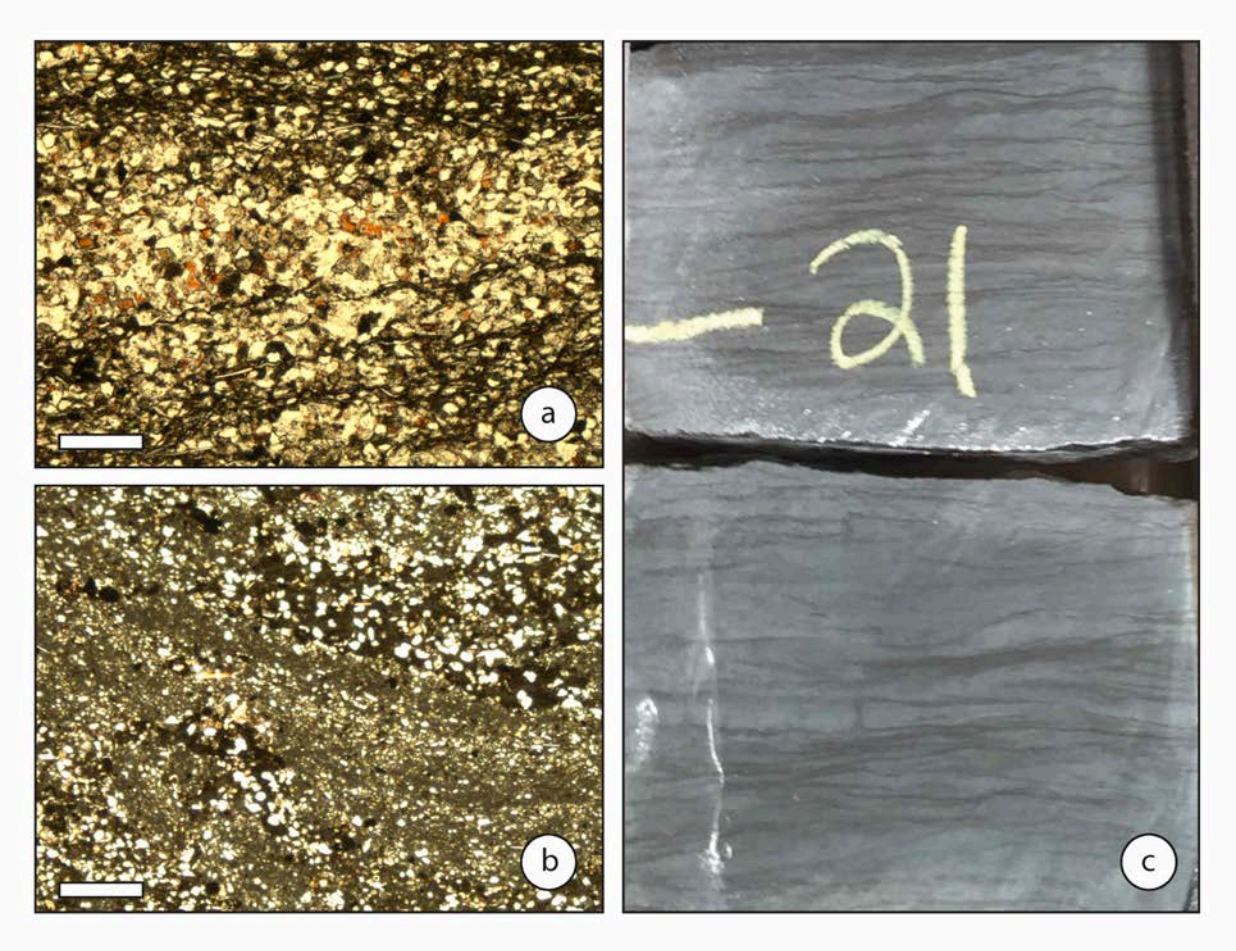

Figure 13. Photomicrographs and core showing examples of facies 6. a) 6822 ft, b) 6773 ft, c) 6821 ft. Images from Tully core. Core slab shows darker drapes of mud and peloids. Scale bar on photomicrographs is 0.5 mm.

Facies 7 – Skeletal grainstone to grain-dominated packstone

Rocks of this facies are characterized by the entire spectrum of post-extinction normal marine invertebrates including low- to high-trochospiral microgastropods, thick-walled prismatic and thin-walled bivalves, scaphopods, rare ammonoids, crinoids, ophiuroids, echinoids, conodonts, calcispheres, serpulid worms, and rare brachiopods. The skeletal material is coarse sand to gravel size and ranges normally from whole (microgastropods, scaphopods, ammonoids, serpulids) to disarticulated (bivalves, brachiopods, echinoderms, conodonts) (Figure 14), although skeletal grains are also subject to variable degrees of breakage and abrasion. The majority of mollusk grains have thin micrite rims and some grains bear thin superficial oolitic coatings. Angular to subangular quartz silt (up to 5%) is a common accessory component of this facies. Peloids with somewhat diffuse margins fill or partially fill shelter and selected interparticle pores. Where partially compacted the peloidal mass takes on a clotted fabric. Further compaction creates a mass of mud wherein distinction of individual peloids is lost. Internal bedding is generally lacking and orientation of elongate grains ranges from horizontal to sub-horizontal, although in some cases elongate grains and skeletal fragments may be vertically oriented. Concentrically arranged silt and microbioclast bands indicate burrowing. Intraparticle pores in gastropods are filled to partially filled with geopetal peloids and mud. Disparity in orientation of geopetal mud indicates redeposition of sediment-filled gastropods or in-place reorientation by burrowing organisms. Most of the original pore space is now filled by calcite cement. Hydrocarbons are often found in the intraparticle porosity.

The large skeletal grains and near absence of carbonate mud in this facies indicates a high-energy environment, such as a mid-ramp shoal front, where fairweather wave action is capable of winnowing the mud without breaking the majority of skeletal grains. Interparticle

pore-reducing and pore-filling peloids may have originated in one of two ways. Since peloids are a common constituent of the Sinbad and Torrey Members, it is likely that many of the peloids are syndepositional fecal pellets. However, it is possible that the peloids with diffuse boundaries occurring in isolated shelter, intraparticle, and some interparticle pores may have resulted from microbially-induced precipitation of micrite-grade peloidal cements.

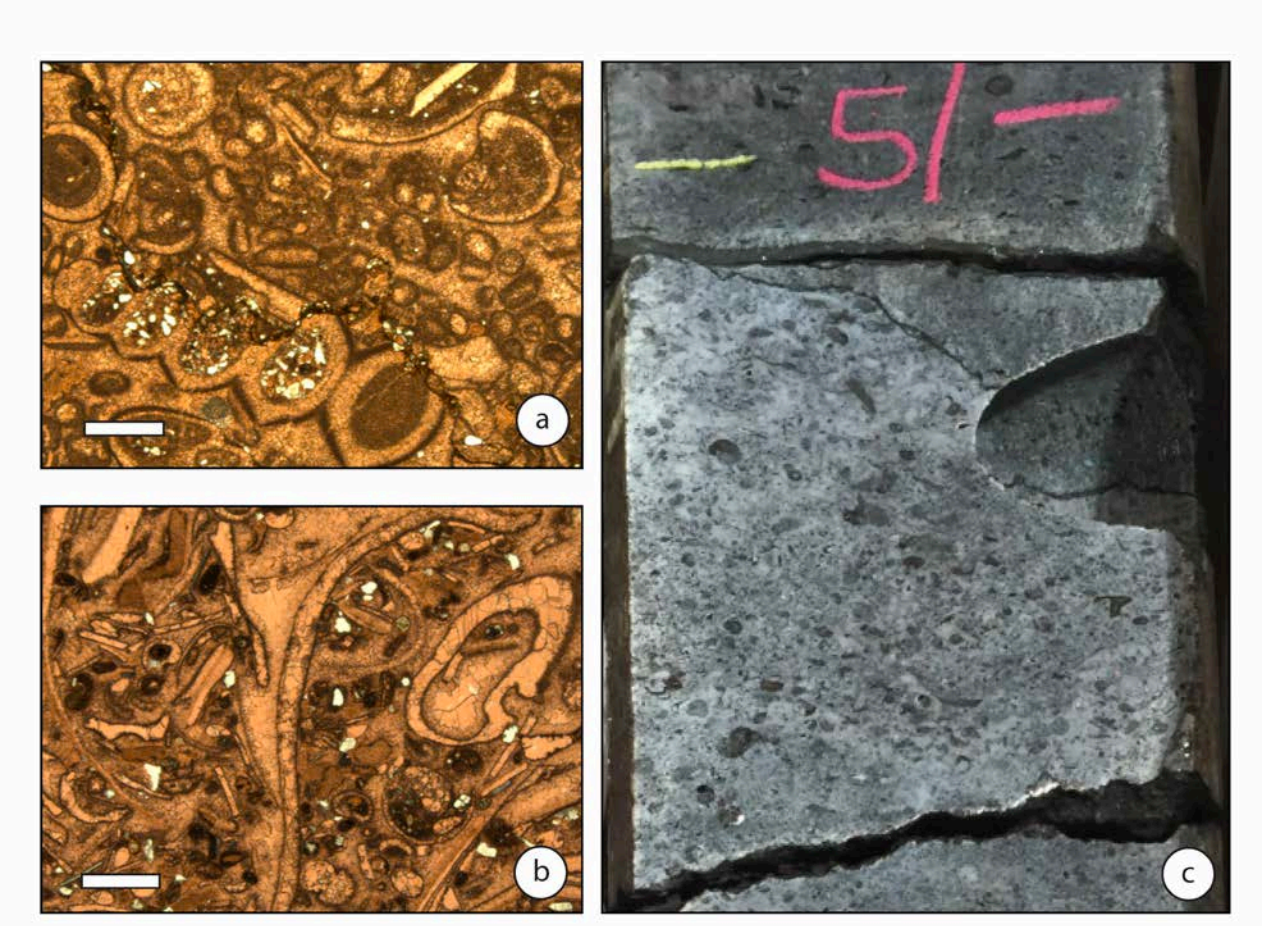

Figure 14. Photomicrographs and core showing examples of facies 7. a) 5724 ft, Wellington Flats core, b) 6845.5 ft, Tully core, c) 6851 ft, Tully core. Core slab shows skeletal texture of this facies. Scale bar on photomicrographs is 0.5 mm.

Facies 8 – Skeletal-peloidal wackestone to packstone

This facies is established for mud- and grain-supported limestone containing ~20% mud, skeletal grains, peloids, and quartz grains (Figure 15). Skeletal constituents include gastropods, bivalves, scaphopods, crinoids, echinoid spines, conodonts, calcispheres, brachiopods, and encrusting organisms. Bivalves, brachiopods, echinoderms, and conodonts are disarticulated. Disarticulated elements range from intact to partially broken. For the most part, gastropods and scaphopods shells are whole and unabraded. Micrite rims are thin and occur sparingly compared to the degree and ubiquity of micrite rims in Facies 7. The matrix is comprised of dense, uniform micrite to microspar. In some cases, the matrix has a clotted fabric suggesting that the packstone texture may have formed through compaction of a peloid-rich matrix. Bedding is generally massive, which along with rotated, geopetal structure indicate pervasive bioturbation.

Rocks of this facies were deposited below fairweather wave base just basinward of the mid-ramp shoal. The presence of mud and general absence of micritization indicates lower energy and lower light levels than the environment in which skeletal packstones and grainstones of Facies 7 were deposited.

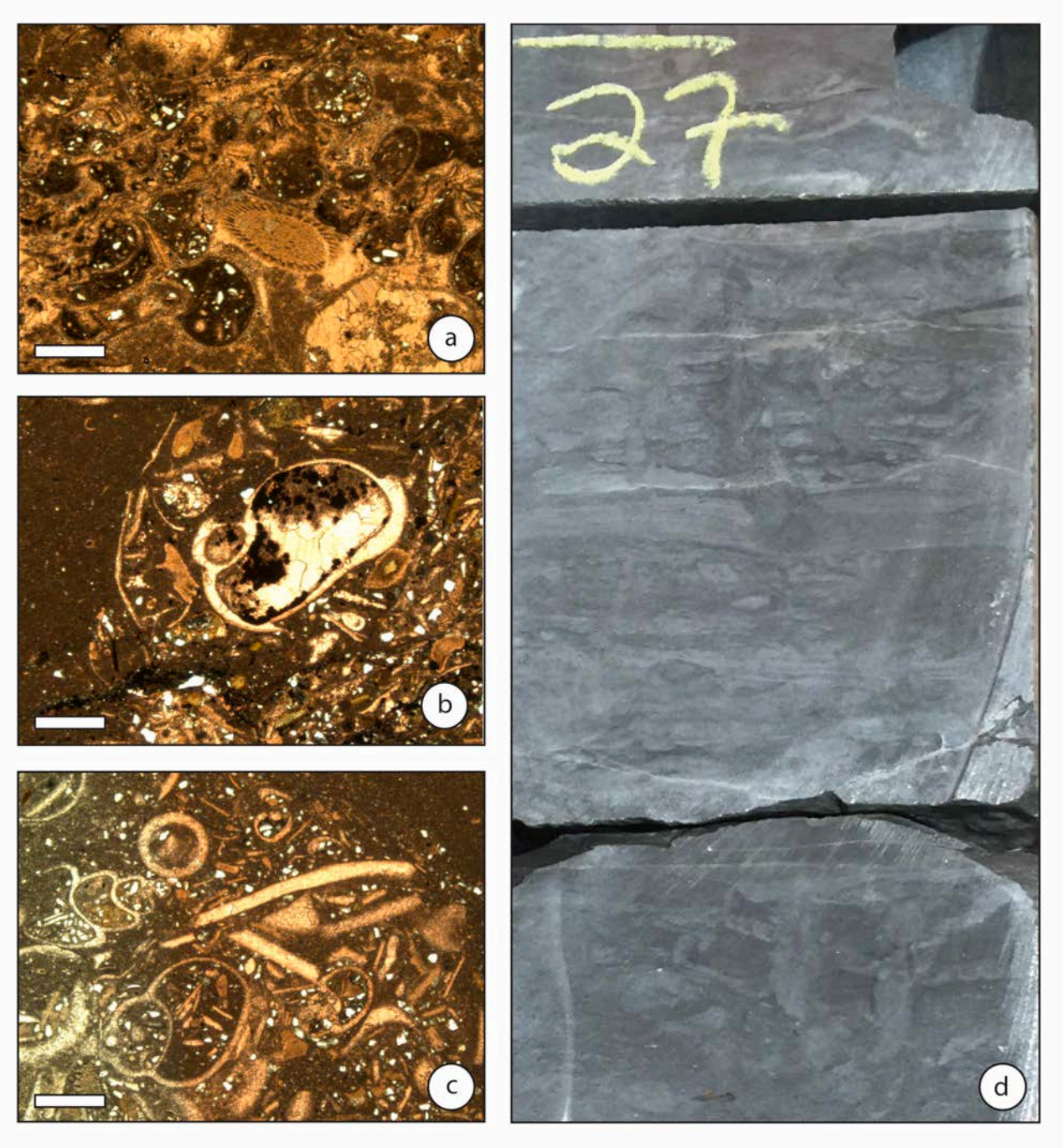

Figure 15. Photomicrographs and core showing examples of facies 8. a) 6824 ft, b) 6790 ft, c) 6833 ft, d) 6827 ft. Images from Tully core. Core slab shows massive sections as well as intraclastic sections. Scale bar on photomicrographs is 0.5 mm.

Facies 9 – Bioclastic-peloidal packstone

Grain-rich carbonate rock containing skeletal bioclasts (40-45%), peloids (25%), mud (10-15%), quartz grains (15%) (Figure 16). Bioclasts are comprised of comminuted fragments of bivalves and gastropods and additional, but unidentifiable invertebrate taxa. Texturally the rocks of this facies are relatively fine grained and moderately well sorted. Rocks of this facies are massive.

The presence of mud, overall fine-grained nature of the sediment, and sorting indicate deposition below fairweather wave base in a position well basinward of the mid-ramp shoal. Bioclasts were formed in the high-energy mid-ramp shoal, then transported along with mud, peloids, and quartz silt to more offshore settings by storms. The shelf was well oxygenated as indicated by pervasive bioturbation of the bottom sediment.

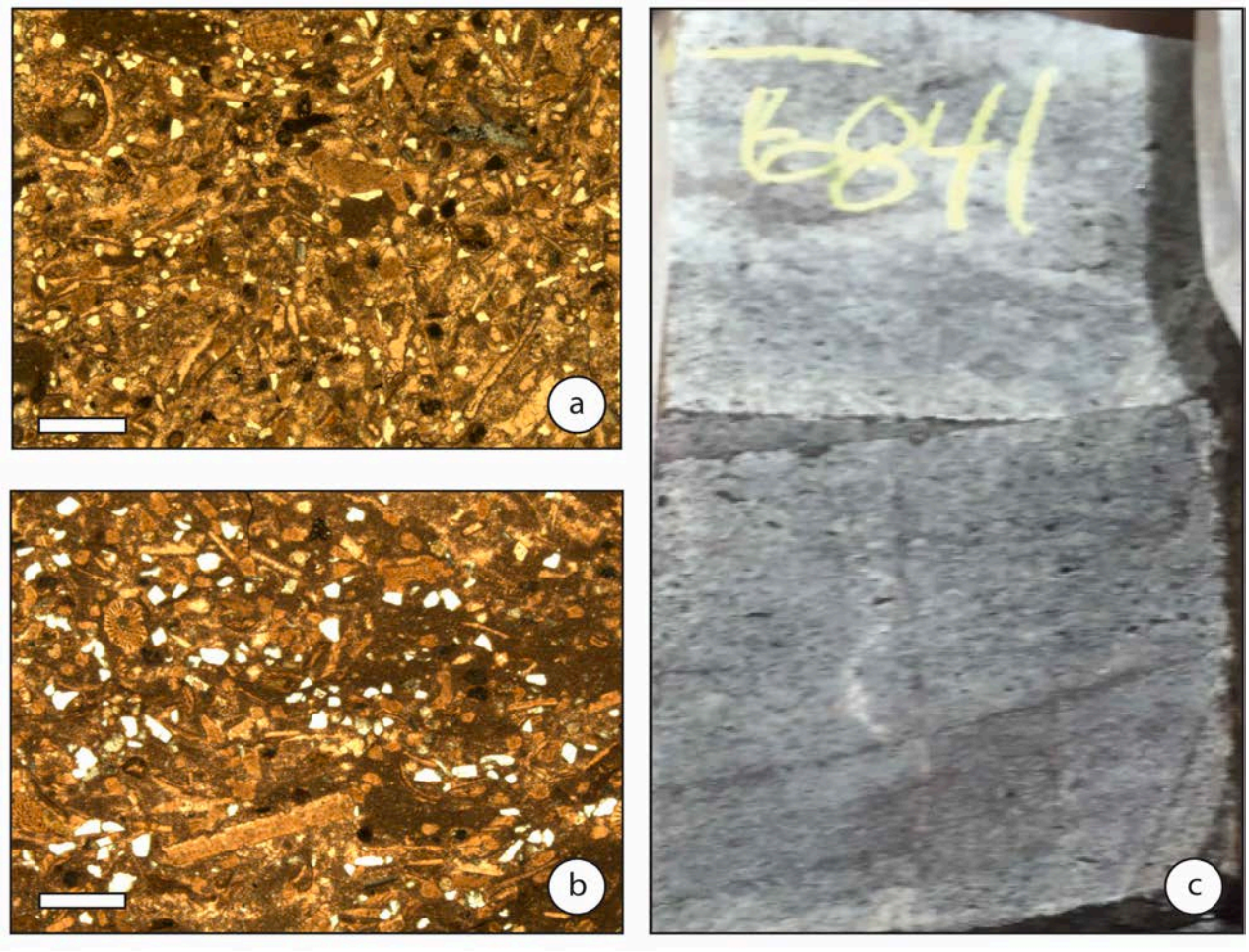

Figure 16. Photomicrographs and core showing examples of facies 9. a) 6850 ft, b) 6834 ft, c) 6841 ft. Images from Tully core. Core slab shows skeletal texture. Scale bar on photomicrographs is 0.5 mm.

Facies 10 – Whole-bivalve-peloid packstone

Carbonate rock containing peloids (70-80%), quartz qrains (5%), and whole bivalve shells (15-25%). Sections of this facies show hummock cross-stratification, while other sections show planar lamination (Figure 17). A distinctive characteristic of this facies is the presence of well-preserved, thin-walled bivalves. Though many of the shells have been disarticuled, individual valves have been preserved to a remarkable degree given the thin walls exhibited by these bivalves. Cement-filled shelter pores associated with these bivalves are also a characteristic

trait. The matrix is light gray in color and is comprised of small, well-sorted peloids. Intraclasts may be present in small numbers in some representatives of this facies.

This facies was deposited in an outer ramp setting where indigenous thin-walled bivalves were able to remain intact. Peloids and small intraclasts, and perhaps much of the matrix settled from suspension in this low-energy setting in the days and weeks following major storms.

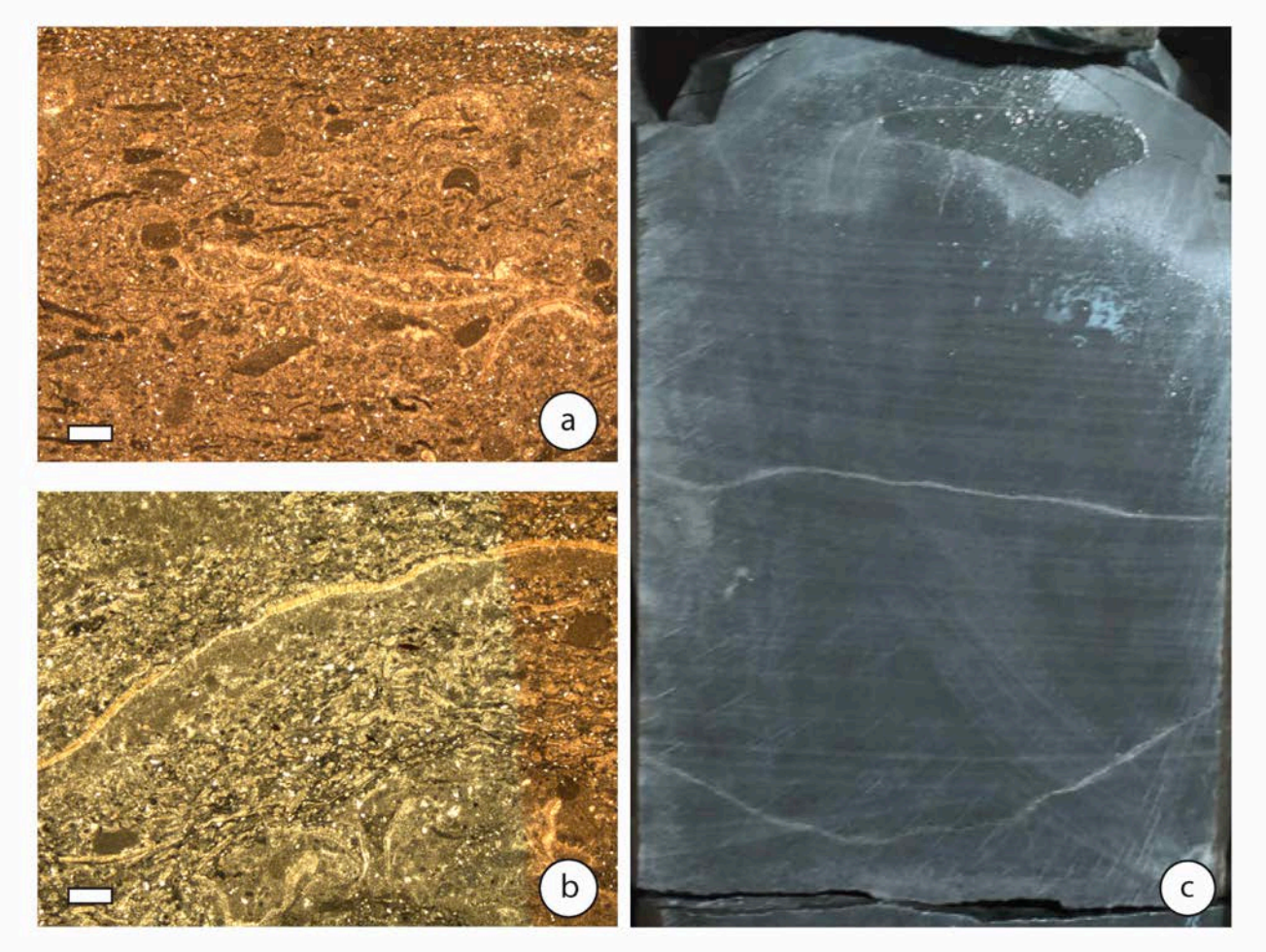

Figure 17. Photomicrographs and core showing examples of facies 10. a) 6808.7 ft, b) 6809.7 ft, c) 6803.5 ft. Images from Tully core. Core slab shows hummocky cross-stratification. Scale bar on photomicrographs is 0.5 mm.

Discontinuity Surfaces

Many discontinuity surfaces are present in the Sinbad Limestone, both in core and in outcrop. A discontinuity surface is any stratigraphic interface where an interruption of sedimentation can be proved (Clari, Pierre, and Martire, 1995). Discontinuity surfaces are crucial in determining the depositional environment and energy regime of a given facies. They also create baffles, impeding the flow of fluids (Shekhar et al., 2014).

Within the Sinbad, discontinuity surfaces can be grouped into three main categories: hardgrounds, firmgrounds, and change surfaces.

Hardgrounds

Carbonate hardgrounds are surfaces of synsedimentarily cemented carbonate layers that have been exposed on the seafloor (Wilson and Palmer, 1992). Evidence of hardgrounds include sharp, linear erosion surfaces, encrusting marine organisms, borings or burrows truncating at the hardground surface, early marine calcite cements, or extensive mineralization of surfaces (Figure 18, Figure 19, Figure 20). Within carbonate rocks, hardgrounds are most common in skeletal grainstones, likely because of the high porosity, permeability, and calcite substrate, and flow-through of marine waters. These features allow for early, extensive cementation (Wilson and Palmer, 1992). Additionally, cementation is most prevalent in the uppermost few centimeters of the carbonate sediment, decreasing downwards (Wilson and Palmer, 1992). In order for hardground to form, a specific horizon must be present at the sediment-water interface for an extended period of time. Therefore, hardgrounds also show evidence of a decrease in the rate of sedimentation, or starved sedimentation.

Thirteen hardgrounds are present throughout the Tully core, all within skeletal grainstones (Figure 4). None were identified in the Wellington Flats core. Fault breccia is present in the only skeletal grainstone in this core, and could have obstructed any hardgrounds present.

Firmgrounds

A firmground indicates stiff but uncemented sediment (Droser et al. 2002). Many scour surfaces were identified in both cores, indicated by deep (1-7cm), jagged, erosive scours. At these horizons, scour usually rips up clasts of the underlying strata, leaving the rip-up clasts suspended above the surface in the overlying, finer grained matrix(Figure 21, Figure 22). For the purposes of this publication, firmgrounds are evidenced by scour and/or rip-up clasts, and are therefore, like hardgrounds, erosional surfaces. The fact that the strata below the surface were deeply and unevenly eroded, along with the presence of rip-up clasts (some of them showing evidence of post-depositional compaction) show that the sediment was compacted, but not yet cemented or lithified. Therefore, these scour surfaces likely represent firmgrounds. Firm sediment conditions generally result from dewatering and compaction (Droser et al. 2002). Therefore, these firmgrounds were likely somewhat buried beneath overlying sediments in order to be compacted and dewatered. Following this shallow burial, an erosive event transported the upper sediments away and eroded into the firm sedimets below, creating the scours and rip-up clasts.

It is possible that firmgrounds without visible scour are present in core, but the scale of this study only allowed for erosive firmgrounds to be studied in detail.

Firmgrounds were identified in both cores, with thirteen in the Tully core, and seven in the Wellington Flats core (Figure 4 and Figure 6). Most of these firmgrounds are present at a

surface that is also a change surface, showing that facies changes were often preceded by a period of erosion.

Change Surfaces

Proposed by Hillgartner (1998), change surfaces represent a change in texture and/or facies without evidence of erosion (Figure 23). These surfaces may represent changes in climate, water depth, energy, or a lateral facies shift. Change surfaces don't necessarily need to show signs of erosion or cementation.

Change surfaces are found in both cores, with twenty being present in the Tully core, and seven in the Wellington Flats core (Figure 4, Figure 6), as there are many more facies changes in the former.

Implications

The frequent occurrence of scour surfaces throughout the Sinbad suggests that, for much of deposition, these carbonates were being deposited on a storm dominated shelf. Great energy would be needed to create as much scour and as many rip-up clasts as are observed in core and outcrop. Sporadic storms would provide the energy needed to create these features. Periods of starved sedimentation must also have occurred in order to create multiple hardgrounds, leaving a horizion of skeletal grains at the sediment-water interface and allowing circulation of water to cement them.

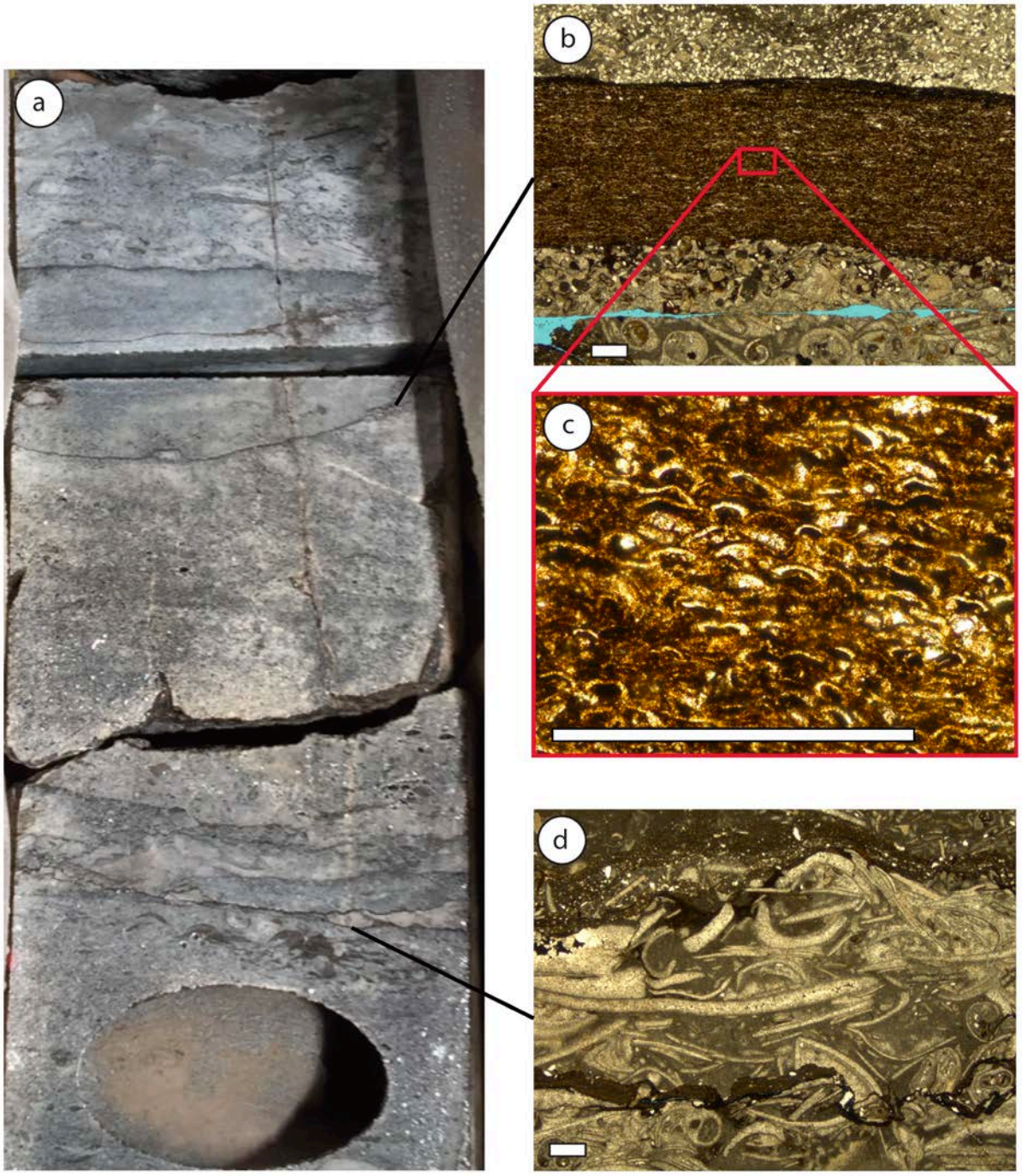

Figure 18. a) Core photograph displaying hardgrounds, Tully core, 6856'; b) Photomicrograph of a hardground with encrusting organisms, Tully core, 6856.3'; c) Zoomed in photograph of encrusters,6856.3'; d) Photomicrograph of additional hardground, Tully core, 6856.7'. Scale bar is 0.5 mm.

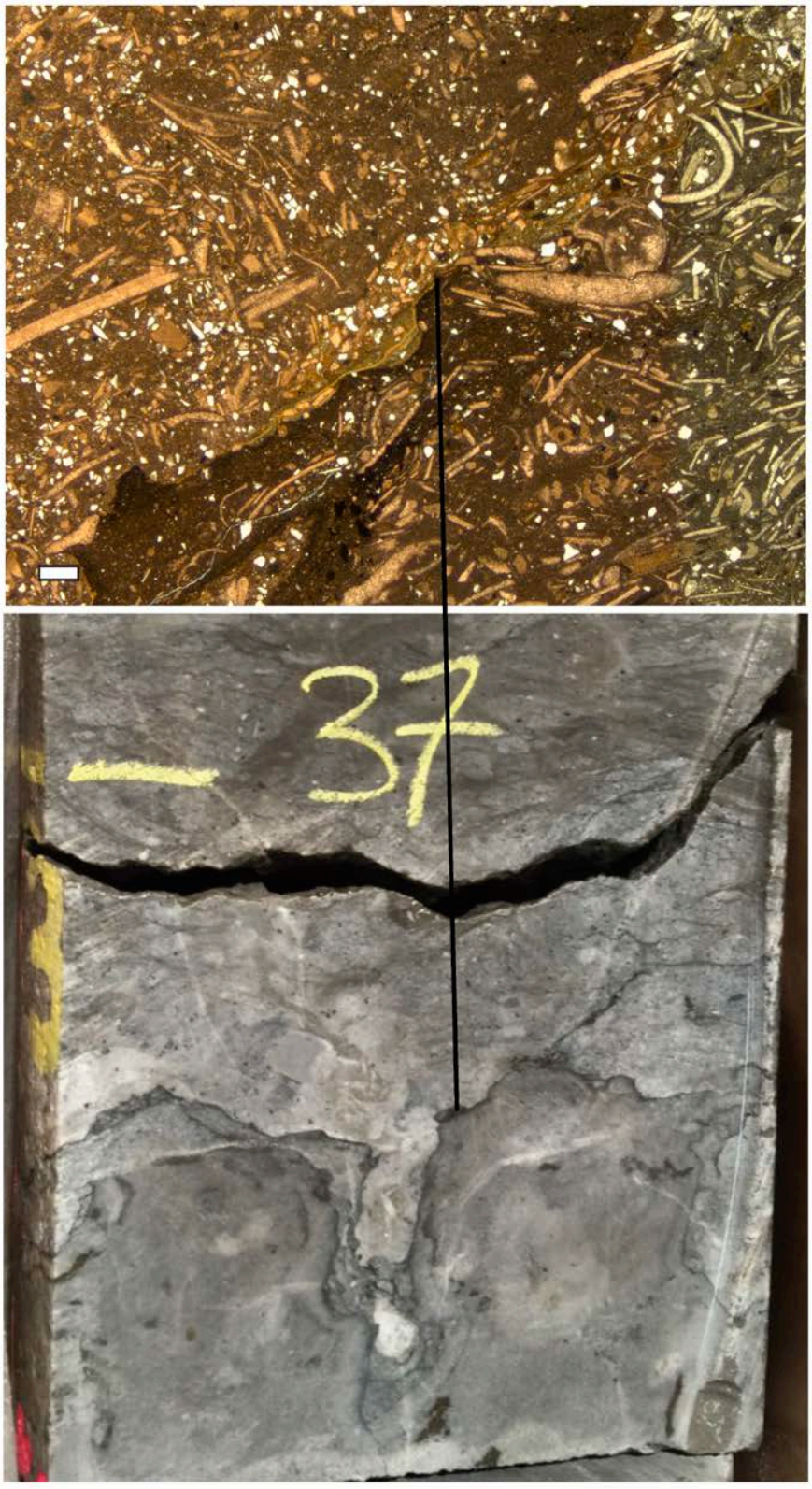

Figure 19. Photomicrograph and core photograph of hardground showing relief, truncated grains, and mineralization, Tully core, 6837'. Scale bar is 0.5 mm.

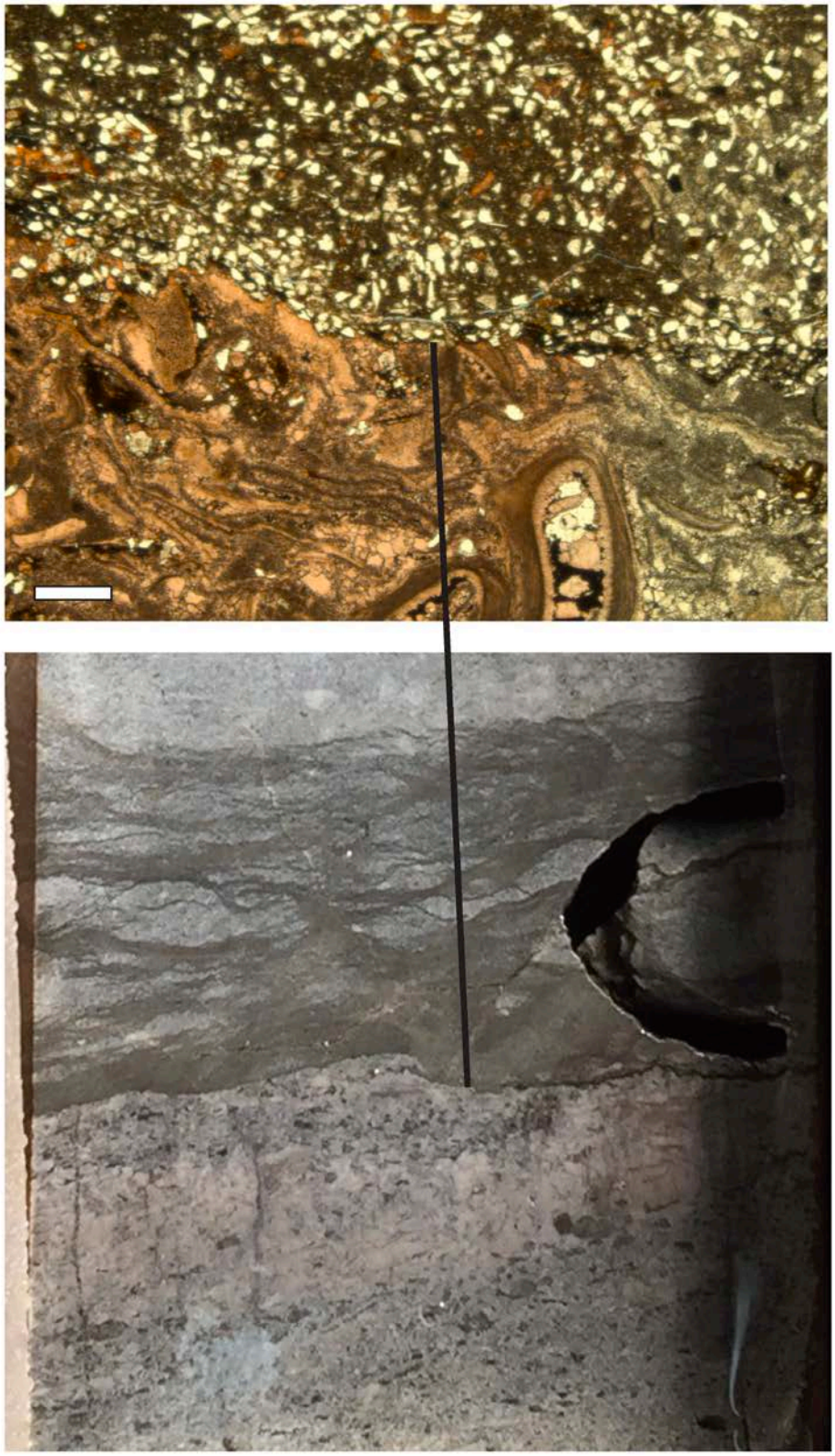

Figure 20. Photomicrograph and core photograph of hardground surface showing truncated skeletal grains and eroisional relief, Tully core, 6852.2'. Scale bar is 0.5 mm.

Figure 21. Photomicrograph and core photograph of firmground showing erosional relief and rip-up clasts, Tully core, 6805'. Scale bar is 0.5 mm.

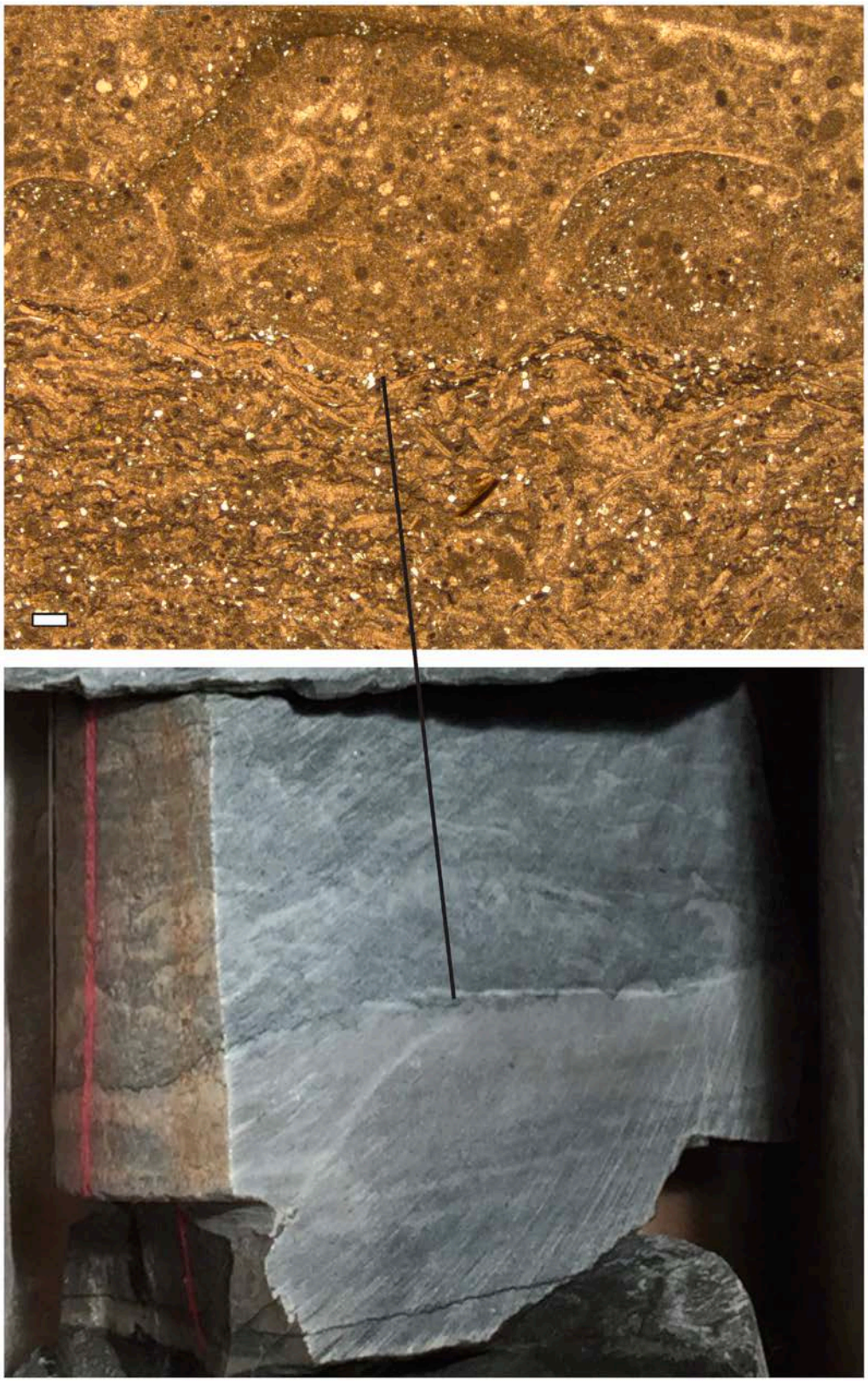

Figure 22. Photomicrograph and core photograph of firmground showing erosional relief, Tully core, 6809.7'. Scale bar is 0.5 mm.

Figure 23. Core photographs showing change surfaces. a) Change in facies, Tully core, 6815'; b) Change in texture, Tully core, 6862'.

Sequence Stratigraphy

The restriction of index fossils (ammonoids and conodonts) to skeletal-rich limestone facies within the Sinbad Member (Brayard et al., 2015) makes it difficult to correlate the broader Moenkopi Formation of east-central Utah with the emerging global Triassic sequence stratigraphic framework of various workers (Aigner and Bachmann 1992, Embry 1997, Posenato, 2008). The ensuing discussion of sequence stratigraphy is therefore necessarily limited

to a treatment of regional and local surfaces and depositional system tracts in the Tully and Wellington Flats cores with allusions to possible wider correlation.

The most widely recognized stratigraphic surfaces of significance to this study are the Tr-1 and Tr-3 unconformities (Papiringos and O'Sullivan 1978), which define the base and top of the Lower Triassic Series throughout the Western Interior, Nevada, and southern California. Marzolf (1993) defined the sedimentary succession between these surfaces as the Moenkopi tectonsequence, but confined his stratigraphic analysis to Lower Triassic outcrops and formations located tens to hundreds of miles south and west of the Wellington Flats, Tully, and Grassy Trial Creek localities. The lithostratigraphy cited by Marzolf (1993) differs from that in the study area, making correlation of subsurface strata to Marzolf's sequence scheme somewhat problematical. Brayard et al. (2015) demonstrated that the Moenkopi tectonosequence reaches a minimum, updip thickness of approximately 185 meters in the San Rafael Swell, compared to thicknesses of over 1000 meters in the Mineral Mountains and Confusion Ranges of western Utah. Smithian-age strata thin from 90 meters in western Utah to a thickness of approximately 20 meters in the San Rafael Swell. Eastward overstepping of successive, onlapping ammonoid zones during the Smithian transgression is largely responsible for this updip thinning of Smithian strata (Brayard et al. 2015). Hence, Lower Triassic strata in the Tully, Wellington Flats, and Grassy Trail Creek cores and in the adjacent San Rafael Swell are relatively thinner and stratigraphically more incomplete than coeval strata in western Utah, Idaho, Nevada, and southern California.

In east-central and southeastern Utah, the Tr-1 unconformity lies between the top of the Early Permian Black Box (Kaibab) Dolomite and base of the Black Dragon Member. This surface reflects a hiatus of nearly 24 million years and displays up to 15 meters of erosional

relief in the San Rafael Swell. In the San Rafael Swell, Goodspeed and Lucas (2007) and Ritter et al. (2013) assigned the Black Dragon through lower Torrey Members to a single third-order depositional sequence. Systems tracts were defined as follows: transgressive systems tract (TST) corresponds to the Black Dragon Member and lower few meters of the Sinbad Member, maximum flooding surface (MFS) corresponds to the skeletal carbonates of the lower Sinbad, the middle and upper Sinbad and lower Torrey represent the highstand systems tract (HST). Likewise, Olivier et al (2013) assigned Black Dragon through Torrey strata near Torrey, Utah to a single third-order sequence with the maximum accommodation corresponding to the *Anisibirites* ammonoid beds that occur in the upper Sinbad Member in their field area. They subdivided the sequence into five "medium-scale sequences" based upon observed stratigraphic relationships. Goodspeed and Lucas (2007) speculated upon the presence of a second sequence boundary at the Sinbad-Torrey contact, but provided no biostratigraphic data to support this conclusion.

With this summary of outcrop-based biostratigraphy and sequence stratigraphy in mind, we now describe the sequence architecture of the subsurface Black Dragon, Sinbad, and lower Torrey Members, beginning with the distal-most Tully core. The Tr-1 surface is placed at a depth of 2223 meters (7296 feet), at the contact between carbonates of the Black Box Dolomite and siliciclasts of the Black Dragon Member. During rise of base level, approximately 20 meters of coarse sandstone and reworked chert-pebble conglomerate (CPC facies of Ochs and Chan, 1990) were deposited on top of the disconformable Tr-1 sequence boundary. Thickness of the basal unit varies with amount of erosional accommodation; thickest where incision was greatest and thinnest atop interfluves. The overlying 55 meters of the Black Dragon Member are composed of interbedded, fine quartz-dominated sandstone, siltstone, and shale (SSS facies of Ochs and Chan,

1990) interpreted to reflect predominantly intertidal sedimentation in response to continued base-level rise. This fine-grained interval is succeeded by an approximately 15 meter-thick succession of trough cross-bedded fluvial deposits (TXS facies of Ochs and Chan, 1990) that indicate a drop in base level and downward shift in coastal onlap. We place a candidate sequence boundary at the base of the sandstone complex and believe that it reflects a break in the more-or-less continuous sea-level rise that began with deposition of the chert-pebble conglomerate. The age of this candidate fourth-order sequence, which we designate as the M1 sequence, cannot be determined biostratigraphically as we did not sample for microfossils. Orgill (1971) reported recovery of conodont specimens from coeval shales of the lower Black Dragon Member in the San Rafael Swell, but the reported taxa are long ranging and provide little age specificity. The age of the candidate M1 sequence could be Greisbachian, Dienerian, or early Smithian. Based on the paleogeographic position of the Tully core, it is unlikely that basal-most Triassic sediments (Greisbachian) were deposited in such a proximal, updip position on the Moenkopi shelf. In Europe and Canada, stratigraphers have recognized distinct Dienerian and Smithian fourth-order sequences separated by a short-lived drop in base level (Aigner and Bachmann 1992, Embry 1997, Posenato, 2008). We propose that the drop in base level indicated by the trough-cross-bedded sandstone complex in the Tully core corresponds with this globally recognized Dinerian-Smithian sea-level drop. Above this candidate sequence boundary, the trough-cross-bedded strata between 2135 meters (7006 feet) and 2153 meters (7066 feet) in the Tully core composes the lowstand systems tract of the overlying upper Dienerian to lower Spathian sequence (which we designate M2) that includes the upper Black Dragon (TST), Sinbad (MFS and lower HST), and lower Torrey (upper HST) Members. Lack of evidence for a hiatus at the Sinbad-Torrey contact in the Tully core argues against placement of a sequence boundary at the contact queried by

Goodspeed and Lucas (2007).

Corresponding sequence stratigraphic surfaces and systems tracts in the Wellington Flats and Grassy Trail Creek cores are shown in Table 2.

		Tully		Wellington Flats		Grassy Trail Creek	
Sequence		meters	(feet)	meters	(feet)	meters	(feet)
M2	HST	2057?-2083	(6750?-6835)	1712?-1741	(5620?-5713)	no data	
	MFS	2083	(6835)	1741	(5713)	1114	(3655)
	TST	2083-2135	(6835-7006	1741-1795	(5713-5890)	1114-1155	(3655-3790)
	LST	2135-2153	(7006-7066)	1795-1804	(5890-5929	1155-1161	(3790-3810)
M1	TST-HST	2148-2223	(7047-7296)	1804-1878	(5929-6162)	1161-1181	(3810-3873)
	Tr-1	2223	(7296)	1878	(6162)	1181	(3873)

Table 2. Depths of significant sequence stratigraphic surfaces in the Sinbad Limestone.

Depositional History

The Sinbad Member was deposited on the west-facing, Early Triassic Sinbad Shelf (Figure 24). As sea level transgressed from the northwest, the region of the Tully core was the first to experience deposition. Microbial mats, tidal deposits, and intraclasts of oolitic limestone are observed in the uppermost units of the Black Dragon Member of the Moenkopi Formation in this core, showing evidence of shallow marine waters. Then, as sea level transgressed further, alternating beds (10 ft) of shallow, lagoonal mudstone and skeletal grainstone were deposited as sea level fluctuated (Figure 25). After these mudstones and skeletal grainstones in the Tully Core, 20 feet of skeletal limestones (grainstones, packstones, wackestones, and bioclastic packstones) were deposited as sea level rose further. This rise in sea level allowed for the deposition of skeletal limestone at the Wellington Flats well, which is further east and landward, where a skeletal grainstone is the first Member of the Sinbad Limestone. Both cores show a

period of deeper water and deposition of skeletal limestone. Eventually, both cores also display an influx of siliciclastics, likely from the progradation of a delta. The resulting siltstone unit contains over 30 feet of hummocks in the Wellington Flats well, but is only 10 feet in the Tully well, further out on the shelf. After this siliciclastic period, sea level transgression or retreat of the delta caused another period of limestone deposition, with ooids being deposited in the Wellington Flats well, and skeletal limestones being deposited further basinward in the Tully Well. These are the last Sinbad units, as the siliciclastic input overpowers carbonate deposition, and both cores display the siliciclastic siltstone of the overlying Torrey Member. The lower units of the Torrey Member are hummocky and contain high percentages of peloids, suggesting that at this position further up on the shelf, the lower section of the Torrey Member is made of marine siliciclastic sediments instead of the terrestrial ones observed higher up stratigraphically and observed further landward in outcrop.

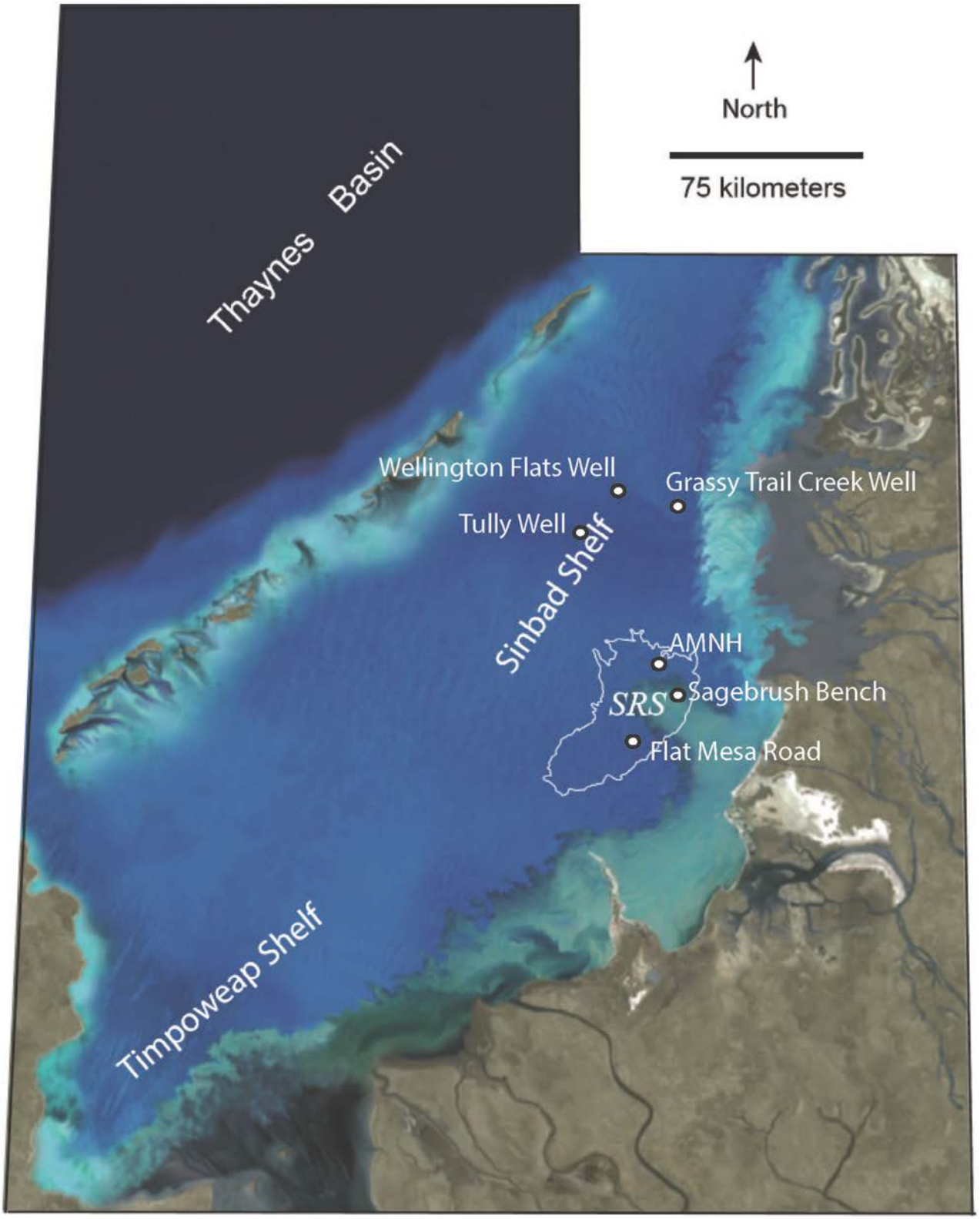

Figure 24. Paleogeographic Map showing Utah in the Early Triassic, with wells and outcrops used in this study superimposed. From Ritter et al. (2013)

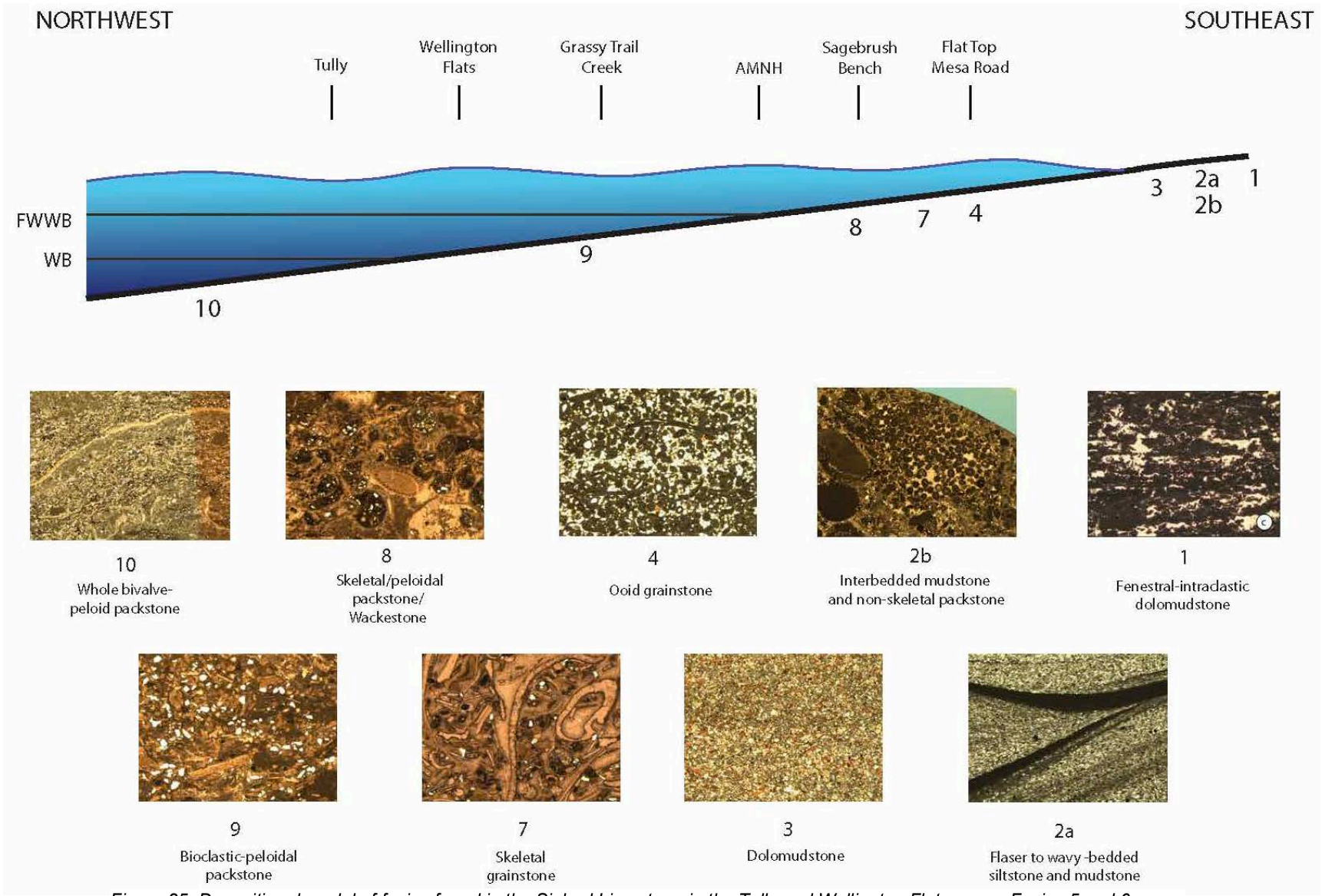

Figure 25. Depositional model of facies found in the Sinbad Limestone in the Tully and Wellington Flats cores. Facies 5 and 6 were excluded as they are dependent on active siliciclastic input. Distances and locations of wells and outcrops are relative and approximate.

Diagenesis

Diagenetic processes have all altered the Sinbad Limestone. The three main diagenetic processes evidenced are seafloor diagenesis, meteoric diagenesis, and burial diagenesis. It is these secondary processes, rather than depositional facies, that primarily determine reservoir characteristics. Diagenesis in the Sinbad Limestone can be observed most readily in alteration to the skeletal grains.

Seafloor Diagenesis

A thin micrite rim is present in most fossil grains (Figure 26c and d). Micritization is caused by endolithic algae boring into the outer layer of carbonate grains. The dark, micrite rim around these grains left by the algae are often the only remaining evidences of skeletal and ooid grains, as other parts of the grain may have been completely dissolved or recrystallized. Neomorphism is present in some fine carbonate muds, creating a crystalline texture (Figure 27a and b). Isopachus fibrous cement is prevalent in grainstones and grain-dominated packstones (Figure 26b and c). This type of cement is typical of marine environments, and it lines almost all of the primary pore spaces, both interparticle and intraparticle. This evidence places the location of micritization and the first episode of cementation in the photic zone within a shallow marine environment.

Meteoric Diagenesis

Effects of meteoric diagenesis are most obvious within the skeletal facies. Exposure to meteoric water is indicated by preferential dissolution of aragonite grains, such as gastropods, scaphopods, and bivalves. Skeletal grains originally made of calcite, such as crinoids,

echinoderm spines, and articulate brachiopods, were not dissolved. In prismatic bivalves, only the aragonite sections were dissolved, leaving the calcite layers unaltered.

The dissolution of aragonite left molds of the skeletal grains, which were then filled with coarse, blocky, sparry calcite that is characteristic of meteoric cementation (Figure 26c and d). This sparry calcite grew on the fine, fibrous cement from the marine cementation, indicating that the meteoric cement occurred after the marine cement. Sparry calcite fills almost all of the pore space that remained after marine cementation. Some of the sparry calcite was dissolved after precipitation, creating some secondary porosity (Figure 26e and f). The presence of cement-filled intraparticle porosity in gastropods and cement-filled shelter porosity in bivalves, along with the overall sparsity of crushed skeletal grains, suggests that cementation occurred before burial.

Carbonate mudstones within the Sinbad Limestone have been completely dolomitized. The fabric of massive, burrowed mudstone is preserved through mimic dolomitization. Dolomite crystals are mostly planar, subhedral rhombs (planar-s), with planar boundaries where crystals meet, and little or no porosity or other material between any crystals (Figure 27e and f). Most oolitic facies have also been dolomitized, and display both fabric-preserving and fabric-destroying dolomitization (Figure 27c and d).

The only diagenesis present in siliciclastic siltstones is calcite cementation. This feature only occurs in the siltstones immediately adjacent to limestone. During meteoric diagenesis, calcite from the limestone was dissolved and redeposited as calcite cement within the siltstones.

Burial Diagenesis

Compaction is evident in most facies. Crushed grains are present in some thin sections (Figure 28a), but are not ubiquitous. Stylolites are present in core, with insoluables lining the

resulting dark bands (Figure 28f). Skeletal grains as well as individual ooids have undergone pressure dissolution, leaving behind jagged edges at suture zones where two skeletal grains or ooids have been crushed together (Figure 28e). Overpacking in all facies in also a sign of deep burial.

During burial stage, hydrocarbons, likely from the underlying Black Dragon Member of the Moenkopi formation, filled pore spaces in many facies (Figure 28c and d). These hydrocarbons were buried deep enough for ambient temperatures to "cook" the kerogen to a high enough maturity to be expelled as oil from the source rock and into the strata of the Sinbad Limestone.

Poikilotopic cement (Figure 29) is present in many of the facies, especially in the Grassy Trail Creek core. Both calcite and anhydrite cement occur as a single, large grain enclosing other carbonate and siliciclastic grains. No boundaries are visible within these poikilotopic cements, other than cleavage planes and twinning. The cement also behaves as a single crystal optically, going extinct in cross polarized light simultaneously.

Boroque (saddle) dolomite is a variety of dolomite that has a warped crystal lattice, and is characterized by curved crystal faces and cleavage, and undulose, sweeping extinction (Figure 28b). Saddle dolomite can be formed both as a result of replacement and void-filling cement. It is precipitated from hydrothermal brines (often between 60 and 150 degrees), and is commonly associated with high levels of sulfates. Because of this, it is often associated with hydrocarbons and is an indicator of burial diagenesis (Radke and Mathis, 1980). Saddle dolomite is found in select sections of the Sinbad Limestone, particularly in the Grassy Trail Creek core.

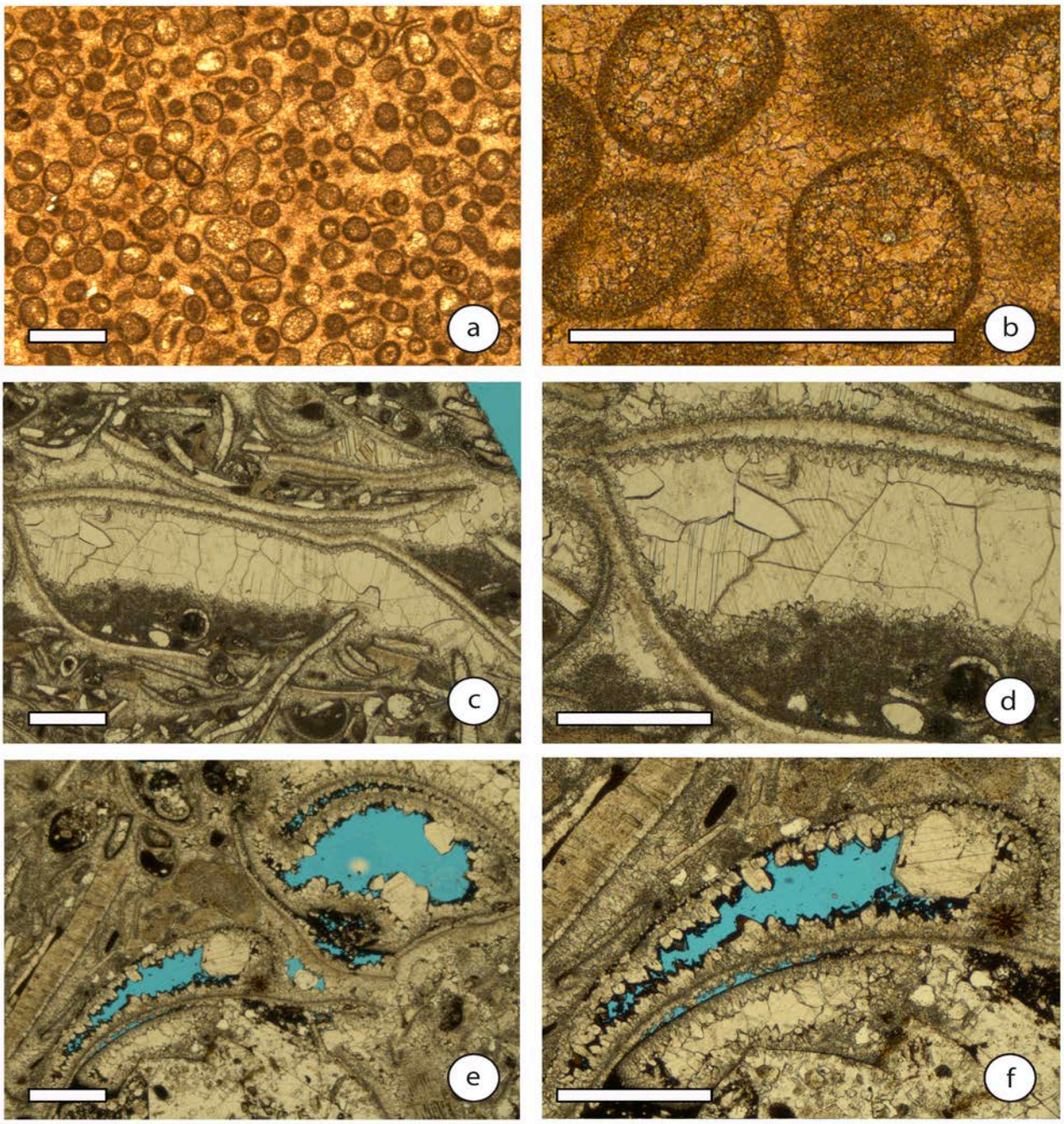

Figure 26. Photomicrographs showing evidence of marine and meteoric diagenesis. a) and b) Micritized and recrystallized ooids, Black Dragon Member, Wellington Flats core, 5727.5'; c) and d) Skeletal grains showing micritization, initial marine cement, and sparry, pore-filling meteoric cement, Tully core, 6845.5'; e) and f) Dissolution of calcite, Tully core, 6851.5. Scale bar is .5mm.

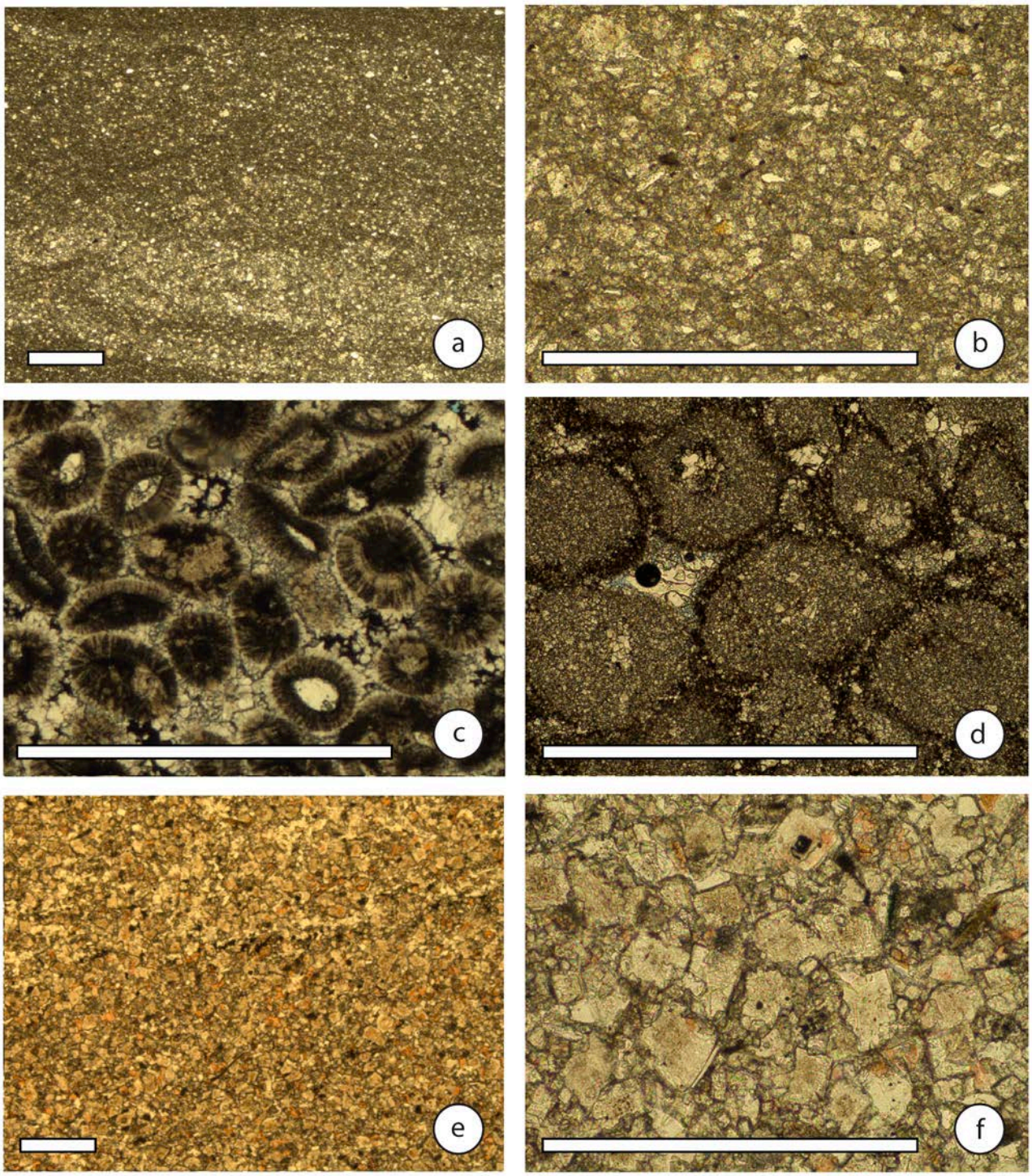

Figure 27. Photomicrographs showing evidence of marine and meteoric diagenesis. a) and b) Neomorphism of carbonate mud, Tully core, 6853.4'; c) Fabric preserving dolomite in ooids, Grassy Trail Creek core, 3630.6'; d) Fabric destroying dolomite in ooids, Tully core. 3608.1'; e) Dolomitization of calcite mud, Tully core, 6862.2'; f) Dolomitization of calcite mud, Tully core, 6862.2'. Scale bar is 0.5 mm.

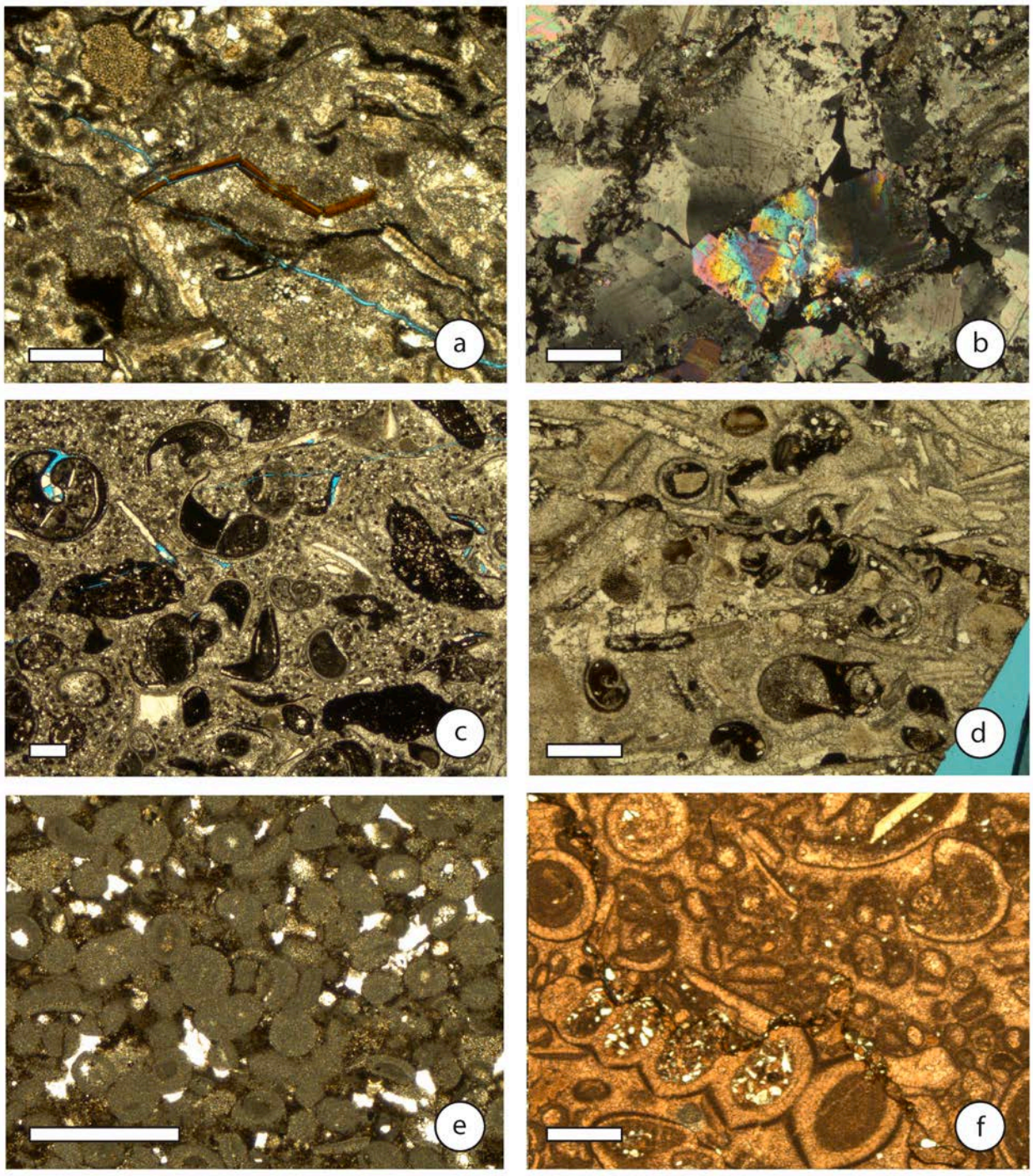

Figure 28. Photomicrographs of evidence of burial diagenesis. a) Crushed inarticulate brachiopod, Grassy Trail Creek core, 3627'; b) Boroque (saddle) dolomite, Grassy Trail Creek core, 3643'; c) Hydrocarbon filled intraparticle pore space, Grassy Trail Creek core. 3624.15'; d) Hydrocarbon filled intraparticle pore space, Tully core, 6791.5'; e) Overpacked and sutured ooids, Grassy trail Creek core, 3594'; f) Stylolite from pressure dissolution, Wellington Flats core, 5724.3'. Scale bar is 0.5 mm.

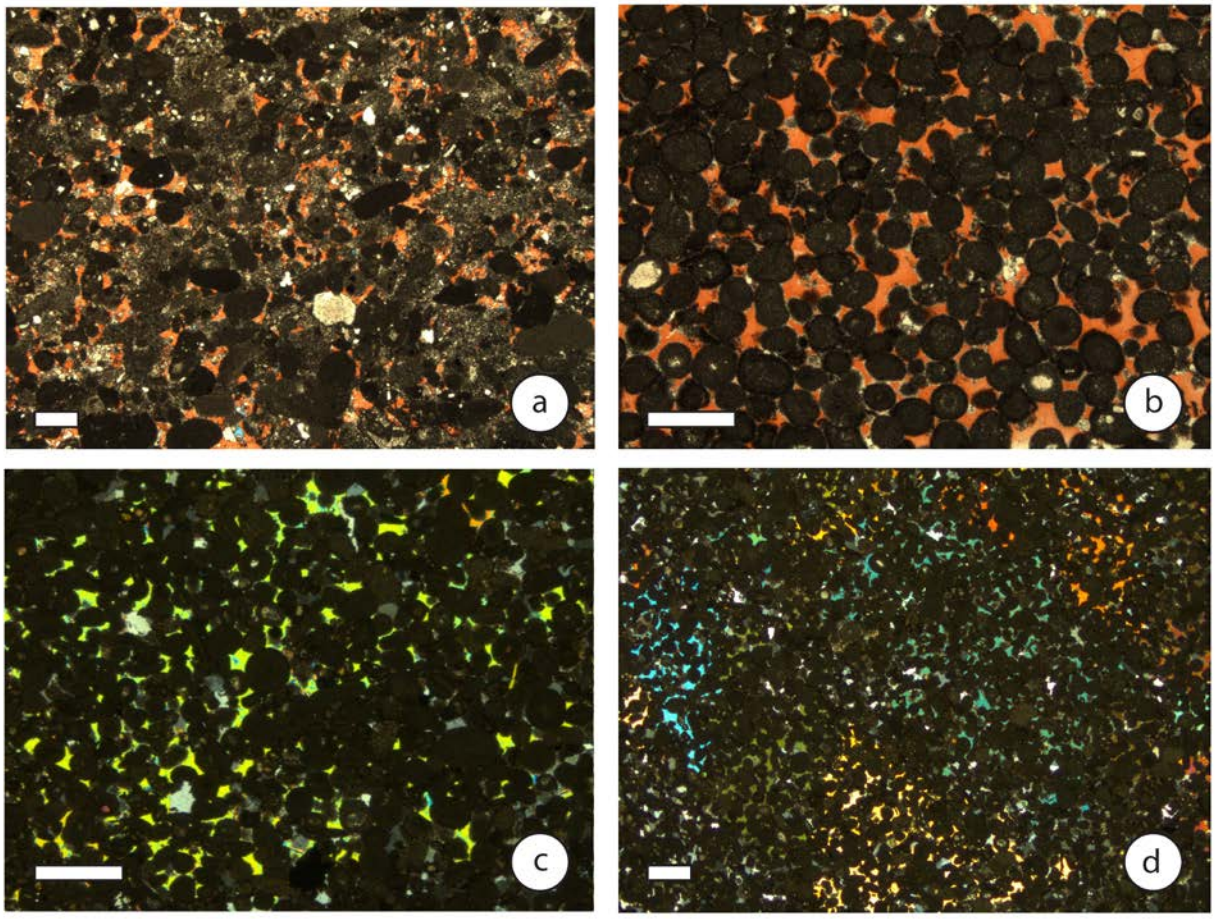

Figure 29. Photomicrographic evidence of poikilotopic cement formed during burial diagenesis. a) Grassy Trail Creek core, 3646'; b) Grassy Trail Creek core, 3605'; c) Grassy Trail Creek core, 3594'; d) Grassy Trail Creek core, 3594'. Scale bar is 0.5 mm.

Porosity and Permeability

Porosity and permeability data were obtained by Whiting Petroleum using core plugs. Each plug with data was classified according to the lithology and plotted accordingly (Figure 30).

The most abundant pore types are interparticle, intraparticle, and moldic pores. Highest values of porosity (8-10%) occur in poorly cemented, quartz-dominated siltstone and dolomitized oolite (Figure 30). Highest values of permeability (.01-1.0 md) also occur within poorly cemented siltstones and dolomitzed oolites. Figure 30 shows that while lithology does exert control over porosity and permeability, many lithologies have similar values, and all facies

have wide ranges and overlap with many other facies. Therefore, rock type itself must not be the main factor that determines porosity and permeability. When the siltstone samples were plotted to differentiate between those with calcite cement and those without, it became clear that almost all siltstones with calcite cement have lower porosity and permeability values than those without calcite cementing the rock. Other rock types also show this relationship between diagenesis and reservoir characteristics (Figure 31). This suggests that diagenesis is the primary factor controlling porosity and permeability.

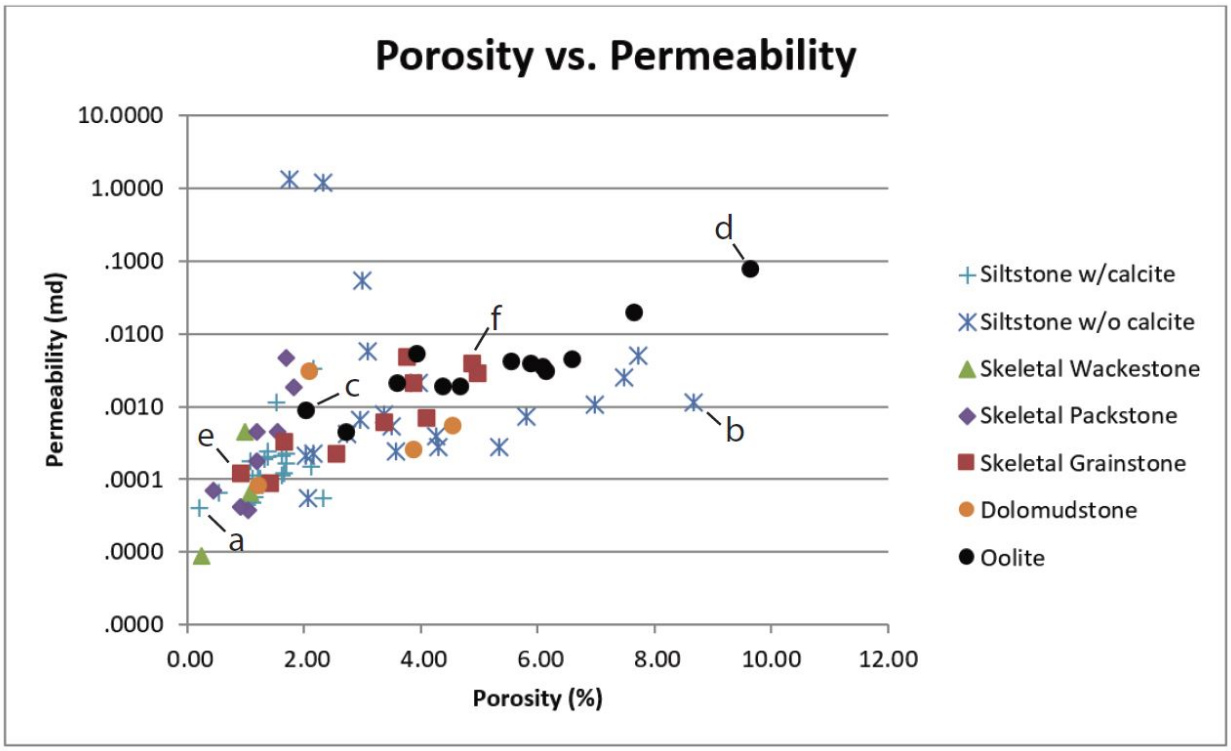

Figure 30. Graph showing the relationship of porosity and permeability of core plugs in both the Tully and Wellington Flats wells according to lithology. Labeled datapoints reference photomicrographs in Figure 31.

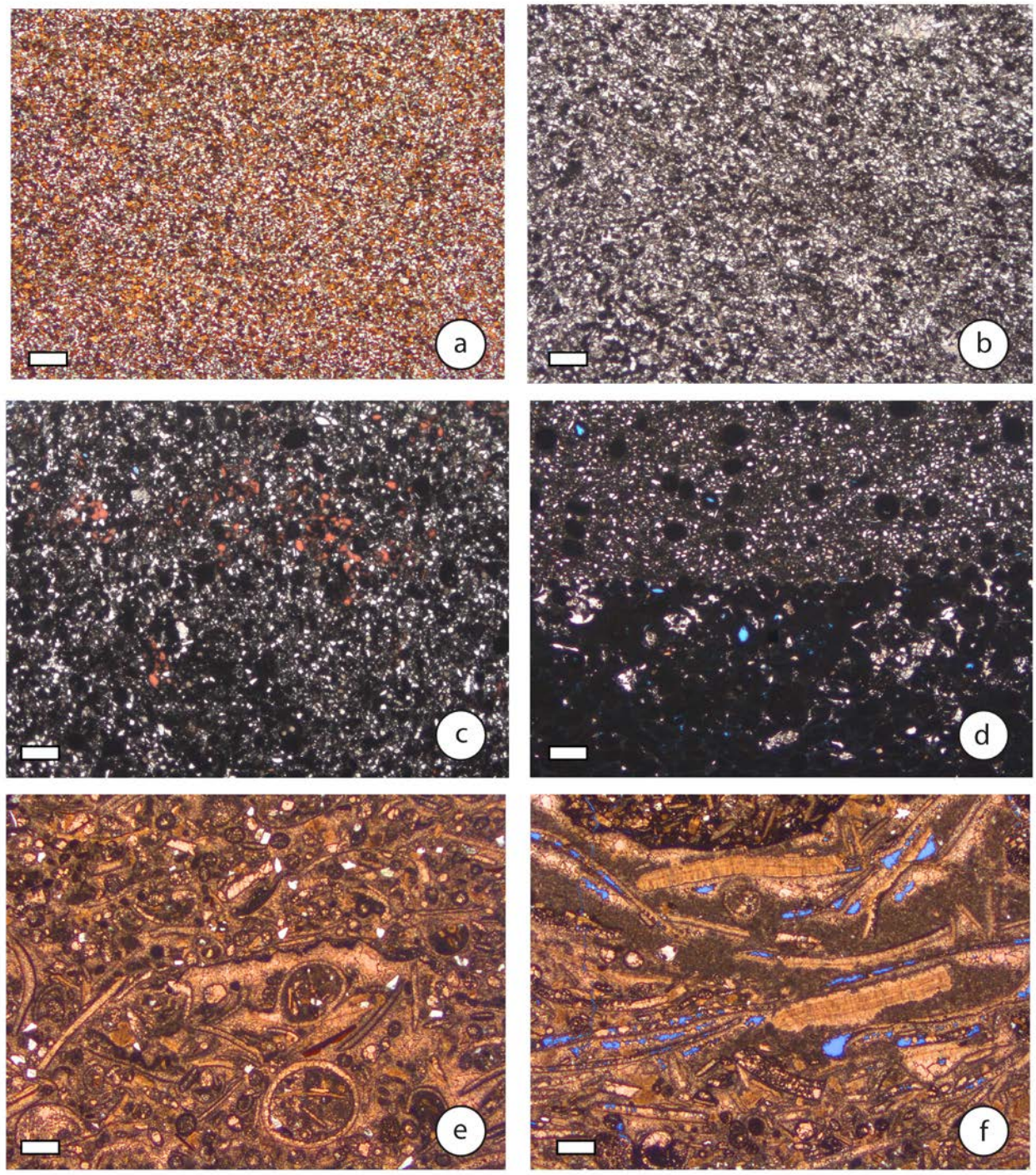

Figure 31. Photomicrographs showing diagenetic features that influence porosity and permeability. Each photomicrograph represents a specific sample labeled on the graph in Figure 30. a) Siltstone with porosity-filling calcite cement, Tully core, 6792.1'. b) Siltstone without calcite cement, Tully core, 6774.5'. c) Oolite with pore-filling calcite cement, Wellington Flats core, 5777.35'. Note micritization of ooids. d) Oolite with moldic and interparticle porosity, Wellington Flats core, 5680.5'. e) Skeletal grainstone showing no visible porosity, Tully core, 6852.9'. f) Skeletal grain-dominated packstone showing moldic and cement-reduced interparticle porosity, Tully core, 6852.1'. Scale bar is 0.5 mm.

CONCLUSIONS

This study, based largely upon the Wellington Flats and Tully cores, extends our understanding of the sedimentology, stratigraphy, and reservoir character of the Lower Triassic (Smithian) Sinbad Limestone Member of the Moenkopi Formation further down depositional dip than afforded by outcrop studies in east-central Utah. The three main units of the Sinbad Limestone Member observed in outcrop (lower, skeletal grainstone; middle, hummocky, peloidal to silty, peloidal packstone; and upper oolitic dolograinstone caprock) are also present in the more proximal Wellington Flats Core. In contrast, skeletal limestone, reflecting deposition in a more distal ramp setting, predominates in the Tully core, which obscures the characteristic threefold subdivision of the Sinbad Limestone.

In core, the Sinbad Limestone Member is composed of seven low-diversity skeletal and nonskeletal carbonate and three siliciclastic or mixed carbonate-siliclastic lithofacies that represent deposition on a storm-dominated carbonate ramp, indicated by common occurrence of hummocky cross bedding, intraclasts, and scour surfaces. Bivalves and micrograstropods, and to a lesser extent crinoids, ophiuroids, scaphopods, ostracodes, and worm tubes are the dominant fossil components. Discontinuity surfaces (hardgrounds, firmgrounds, and change surfaces), particularly in the skeletal limestone intervals, reveal that sedimentation was slow and punctuated by periods of non-deposition, some accompanied by cementation (hardgrounds) of the seafloor. A complete understanding of the sequence stratigraphy of the studied interval is obscured by lack of critical biostratigraphic data. The Black Dragon through lower Torrey members have been grouped into a single 3rd-order sequence by previous authors (Goodspeed and Lucas, 2007; Ritter et al., 2013) with the Sinbad Limestone representing the maximum-flood facies. However, stacked fluvial channels in the middle of the Black Dragon Member may

indicate an intra-Black Dragon lowstand that warrants recognition of an additional, possibly Greisbachian-age 3rd-order sequence consisting of the lower half of the Black Dragon Member.

The Sinbad Limestone has been subjected to a range of diagenetic modifications associated with marine, meteoric, and burial processes. Seafloor diagenesis can be observed in micritization of skeletal grains and marine cements. Meteoric diagenesis is evidenced by pore-occluding and pore-filling sparry calcite cement and by the presence of moldic pores. Crushed grains and poikilotopic cement are evidence of burial diagenesis. The highest values of porosity (8-10%) and permeability (.01-1.0 md) occur in poorly cemented siltstones and dolomitized oolites. Diagenesis is the main factor that ultimately determines reservoir characteristics.

REFERENCES

Batten, R. L., & Stokes, W. L.,1986, Early Triassic gastropods from the Sinbad Member of the Moenkopi Formation, San Rafael Swell, Utah: American Museum of Natural History.

Bebout, D.G., and Loucks, G.G., 1984, Handbook for logging carbonate rocks: Bureau of Economic Geology Handbook 5, Austin, Texas, 43pp.

Blakey, R.C., 1973, Stratigraphy and origin of the Moenkopi Formation (Triassic) of southeastern Utah: Mountain Geologist, v. 10, p. 1-17.

Blakey, R.C., 1974, Stratigraphic and depositional analysis of the Moenkopi Formation, southeastern Utah: Utah Geological and Mineralogical Survey Bulletin 104, 81 pp.

Boyer, D.L., Bottjer, D.J., and Droser, M.L., 2004, Ecological signature of Lower Triassic shell beds of the western United States: Palaios, v. 19, p. 372-380.

Brayard, A., Bylund, K.G., Jenks, J.F., Stephen, D.A., Olivier, N., Escarguel, G., Fara, E., Vennin, E.,2013, Smithian ammonoid faunas from Utah: implications for Early Triassic biostratigraphy, correlation and basinal paleogeography: Swiss Journal of Paleontology, v. 132, p. 141–219

Clari, P.A., Dela Pierre, F., Martire, L., 1995, Discontinuities in carbonate successions: identification, interpretation and classification of some Italian examples: Sedimentary Geology v. 100, p. 97 – 121.

Dean, J. S., 1981, Carbonate petrology and depositional environments: of the Sinbad Limestone Member of the Moenkopi Formation in the Teasdale Dome Area, Wayne and Garfield Counties, Utah (Master's thesis, Brigham Young University).

Dunham, R. J., 1962, Classification of carbonate rocks according to depositional texture, in W. E. Ham, ed. Classification of carbonate rocks—a symposium: American Association of Petroleum Geologists Memoir 1, p. 108- 121.

Dott, R. H., JR., 1964, Wacke, graywacke and matrix: Journal of Sedimentary Petrology, v. 34, p. 625-632.

Droser ML, Jensen S, Gehling JG., 2002, Trace fossils and substrates of the terminal Proterozoic–Cambrian transition: Implications for the record of early bilaterians and sediment mixing. Proceedings of the National Academyof Sciences, USA v. 99:12572–76.

Fraiser, M.L., and Bottjer, D.J., 2000, The U-shaped trace fossil Arenicolites: Burrow of an opportunist during the biotic recovery from the end-Permian mass extinction: Geological Society of America Abstracts with Programs, v. 32, 7, p. 368.

Gilluly, James, and Reeside, J. B. Jr., 1928, Sedimentary rocks of the San Rafael Swell and some adjacent areas in eastern Utah: U. S. Geological Survey Professional Paper 150-D, p. 61-110.

Goodspeed, T.H. and Lucas, S.G., 2007, Stratigraphy, sedimentology, and sequence stratigraphy of the Lower Triassic Sinbad Member, San Rafael Swell, Utah. In: S.G. Lucas and J.A. Spielmann (eds.), Triassic of the American West. New Mexico Museum of Natural History and Science Bulletin, v. 40, p. 91–102.

Hautmann, M. and Nutzel, A., 2005, First record of a heterodont bivalve (Mollusca) from 42 the Early Triassic: Palaeoecological significance and implications for the 'Lazarus Problem': Palaeontology, v. 48, p. 1131-1138.

He, Y. and Gao, Z., 1999, The characteristics and recognition of internal-tide and internal-wave deposits. Chinese Science Bulletin, v. 44(7), p.582-589.

Hunt, C.B., 1953, Geology and geography of the Henry Mountains region, Utah: U.S. Geological Survery Professional Paper 228, 234 pp. Hillgartner, H., 1998. Discontinuity surfaces on a shallowmarine carbonate platform (Berriasian, Valanginian, France and Switzerland). Journal of Sedimentary Research, v. 68, p. 1093–1108.

Jackson, A.L., 1993, Last Chance, South: In Hill, B.G. and S.R. Bereskin (eds.), Oil and Gas Fields of Utah, Utah Geological Association Publication, v. 22, 6 pp.

Lehrmann, D.J., Ramezani, J., Bowring, S.A., Martin, M.W., Montgomery, P., Enos, P., Payne, J.L., Orchard, M.J., Hongmei, W. and Jiayong, W., 2006, Timing of recovery from the end-Permian extinction: Geochronologic and biostratigraphic constraints from south China. Geology, v. 34(12), p.1053-1056.

Lucia, F.J., 1995, Rock-fabric petrophysical classification of carbonate pore space for reservoir characterization. American Association of Petroleum Geologists Bulletin, v. 79, p. 1275–1300.

Lutz, S. J., 1993, Sequence stratigraphic interpretation of a mixed carbonate-siliciclastic shelf environment: The Triassic Moenkopi Formation in central Utah: American Association of Petroleum Geologists, Abstract, Rocky Mountain Sectional Meeting, v. 77, p. 1454.

Lutz, S. J., and Allison, M.L., 1992, Geology of the Grassy Trail Creek Field, Carbon and Emery counties, Utah: Utah Geological Survey Contract Report 92-3, 36 pp.

Marzolf, J.E., 1994, Reconstruction of the early Mesozoic Cordilleran cratonic margin adjacent to the Colorado Plateau, in Caputo, M.V., Peterson, J.A., and Franczyk, K.J., eds., Mesozoic systems of the Rocky Mountain region, USA: Denver, Rocky Mountain Section SEPM, p. 181-215

Marzolf, J. E. 1993, Sequence-stratigraphic relationships across the palinspastically reconstructed Cordilleran Triassic cratonal margin. In, Lucas, S. G. & Morales, M. (eds) The nonmarine Triassic. New Mexico Museum of Natural History Bulletin 3, 331–43. Albuquerque: New Mexico Museum of Natural History and Science.

Mathis, A. C., 2000, Capitol Reef National Park and Vicinity Geologic Road Logs, Utah, in: P.B. Anderson and D.A. Sprinkel (eds.) Geologic Road, Trail, and Lake Guides to Utah's

Parks and Monuments Utah Geological Association Publication 29. http://www.utahgeology.org/uga29Titles.htm.

Nutzel, A., and Schulbert, C., 2005, Facies of two important Early Triassic gastropod lagerstatten: Implications for diversity patterns in the aftermath of the end Permian mass extinction: Facies, v. 51, p. 480-500.

Ochs, S. and Chan, M. A., 1990, Petrology, sedimentology and stratigraphic implications of Black Dragon Member of the Triassic Moenkopi Formation, San Rafael Swell, Utah: The Mountain Geologist, v. 27, p. 1-18.

Olivier, N., Brayard, A., Fara, E., Bylund, K.G., Jenks, J.F., Vennin, E., Stephen, D.A. and Escarguel, G., 2014, Smithian shoreline migrations and depositional settings in Timpoweap Canyon (Early Triassic, Utah, USA): Geological Magazine, v. 151(05), p. 938-955.

Olivier, N., Brayard, A., Vennin, E., Escarguel, G., Fara, E., Bylund, K.G., Jenks, J.F., Caravaca, G. and Stephen, D.A., 2015, Evolution of depositional settings in the Torrey area during the Smithian (Early Triassic, Utah, USA) and their significance for the biotic recovery: Geological Journal, v. 51, p. 600-626.

Porter, M.L., 1991, Sequence stratigraphic framework of arid basin deposits: Examples from the Triassic and Jurassic of the San Rafael Swell and adjacent areas, east-central Utah: Geological Society of America Abstracts with Programs, v. 23, p. 90.

Radke, B.M., Mathis, R.L., 1980, On the formation and occurrence of saddle dolomite: Journal of Sedimentary Petrology, v. 50, p. 1149–1168.

Reineck, H. E. and Wunderlich, F., 1968, Classification and origin of flaser and lenticular bedding: Sedimentology, v. 11, p. 99-104.

Ritter, S.M., 2009, May. Sedimentary Petrology and Reservoir Character of a Post-Extinction Carbonate Platform: The Early Triassic (Smithian) Sinbad Limestone Member of the Moenkopi Formation, Utah. In Geological Society of America Abstracts with Programs, v. 41, p. 37).

Stephen, D.A. Bylund, K.G., Bybee, P.J., Ream, W.J., 2010, Ammonoid beds in the Lower Triassic Thaynes Formation in Western Utah, USA, In Tanabe, K. Shigeta, Y, Sasaki, T., and Hirano, H. (eds) *Cephalopods – Past and Present,* Tokai University Press, Tokyo, p. 243-252.

Schubert, J.K., and Bottjer, D.J., 1995, Aftermath of the Permian-Triassic mass extinction event: Paleoecology of Lower Triassic carbonates in the western USA: Palaeogeography, Palaeoclimatology, Palaeoecology, v. 116, p. 1-39.

Shekhar R., Sahni I., et al. 2014, Modelling and simulation of a Jurassic carbonate ramp outcrop, Amellago, High Atlas Mountains, Morocco: Petroleum Geoscience, v. 20, 109–124.

Smith, J.F., Huiff, L.C., Hinrichs, E.N., and Leudke, R.B., 1963, Geology of the Capitol Reef area, Wayne and Garfield Counties, Utah: U.S. Geological Survey Professional Paper 363, 102 pp.

Twitchett, R.J., Feinberg, J.M., O'Connor, D.D., Alvarez, W., and McCollum, L.B., 2005, Early Triassic Ophiuroids: Their paleoecology, taphonomy, and distribution: Palaios, v. 20, p. 213-223.

Twitchett, R.J., 1999, Palaeoenvironments and faunal recovery after the end-Permian mass extinction: Palaeogeography, Palaeoclimatology, Palaeoecology, v. 154, p. 27–37.

Wilson, M.A.; Palmer, T.J., 1992, "Hardgrounds and hardground faunas": University of Wales, Aberystwyth, Institute of Earth Studies Publications 9, p. 1–131.